IEEE Access
Multidisciplinary | Rapid Review | Open Access Journal

Received 13 May 2025, accepted 8 July 2025, date of publication 14 July 2025, date of current version 18 July 2025.

Digital Object Identifier 10.1109/ACCESS.2025.3588595

RESEARCH ARTICLE

Comparative Study of Disturbance Observer-Based Control Methods on an Industrial Gimbal System

MÜCAHİD RIDVAN KAPLAN[1,2], BURAK KÜRKÇÜ[3], (Member, IEEE), MEHMET ÖNDER EFE[2], (Senior Member, IEEE), AND ZEKİ YAĞIZ BAYRAKTAROĞLU[4]

[1]Control Systems Design Department, Aselsan Inc., Akyurt, 06750 Ankara, Türkiye
[2]Department of Computer Engineering, Hacettepe University, 06800 Ankara, Türkiye
[3]Department of Electrical and Computer Engineering, Santa Clara University, Santa Clara, CA 95053, USA
[4]Department of Mechanical Engineering, Istanbul Technical University, Beyoğlu, 34437 Istanbul, Türkiye

Corresponding author: Mücahid Rıdvan Kaplan (mrkaplan@aselsan.com)

This work was supported in part by Aselsan Inc.

ABSTRACT Disturbance-observer-based control (DOBC) methods are developed to approximate the closed-loop behavior of dynamic systems to the nominal system response determined during the design phase. In the literature, many different approaches have been derived for similar purposes. This paper presents a comprehensive experimental evaluation of notable DOBC structures, conducted in both a simulation environment with a comparative analysis and in real-time experiments. Unlike previous studies, which predominantly focus on theoretical analysis or simulation-based assessments, this study provides a systematic experimental comparison of DOBC methods implemented on a gimbal platform, offering insights into their practical performance. For this purpose, the mathematical representations of the DOBC methods have been rearranged in an application-oriented framework and employed for high-precision control of a gimbal platform. A dedicated simulation environment has been established to enable a proper comparison of the proposed DOBC methods in terms of applicability and performance evaluations, considering well-defined and measurable metrics within the experimental setup. The control system designs based on the methods evaluated in this paper were carried out in line with the original studies as originally suggested. The results of the investigation are interpreted using both time- and frequency-domain metrics, highlighting the practical implications of DOBC methods in real-world applications.

INDEX TERMS Disturbance observer, estimation, gimbal, observer, performance, robustness, uncertainties.

NOMENCLATURE

Parameters

Δ	Stable unstructured uncertainty function satisfying.
Δ_A	Unknown state matrix.
Δ_B	Unknown control matrix.
η	Learning rate.
$\mathbb{R}$	Set of the real number.
$\tilde{G}(s)$	Actual plant.
A	Known state matrix.
A_m	Known state matrix of the reference system.
B	Known control matrix.
b	Viscous friction coefficient.
B_d	Control input channel where is disturbance $d(t)$ injected thought.
B_m	Known control matrix of the reference system.
$C(s)$	Main controller.
C	Output matrix.
D	Direct transition matrix.
$G(s)$	Nominal plant model.
I	Identity matrix.

The associate editor coordinating the review of this manuscript and approving it for publication was Lei Wang.

J	Moment of inertia of the system.
K	State feedback gain.
k	Relative degree of the transfer function.
K_e	Error feedback gain matrix.
L, L_x	Observer gain matrix.
$Q(s)$	Q-Filter.
$S(s)$	Sensitivity function.
$s, j\omega$	Complex frequency variable in Laplace domain.
$T(s)$	Closed-loop transfer function or complementary sensitivity function.
W_T	Robustness weight function.

Variable

$\hat{d}$	Estimated disturbance.
$\hat{x}$	Estimated state vector.
$\hat{y}$	Estimated output vector.
d	External disturbance.
d_l	Lump disturbance.
d_{ed}	Equivalent disturbance.
r	Reference vector of the system.
u	Control signal where is related action transmitted by the controller.
u_{tot}	Effective control signal.
x	State vector.
x_m	State vector of the reference system.
y	Output vector of the system.

I. INTRODUCTION

The advancements in science and technology, which have grown exponentially in recent years, also enhanced the demand for the performance and stability expected from the resulting engineering systems [1]. This situation leads researchers working on control theory, like other engineering fields, to search for stable, high-performance methods. The complexity of physical phenomena taking place in advanced engineering systems makes it challenging to represent dynamic behavior with precise physics-based models. In real-world scenarios, in addition to the challenges of obtaining precise information about exogenous disturbances, accurately capturing the behavior of a complex system with a physics-based model necessitates the consideration of uncertainties, even when the system appears to display certainty. Thus, recovering nominal performance under disturbances and dynamic uncertainties in feedback systems is a focal point for researchers seeking to address it within a control theoretical framework. For instance, introducing feed-forward action can enhance the closed-loop performance, assuming that there is no uncertainty and that the disturbances are known [2], although these assumptions are hardly met in practice [3].

Despite the structural similarities between feedforward control and disturbance observer-based (DOB) control [4], there is a growing interest in favor of DOB control [5]. The works by Ohnishi et al. [6] and independently by Johnson [7] are considered the first instances of disturbance observer-based control (DOBC) system design. Following these pioneering ideas, more advanced examples of DOB control have emerged and spread across various fields over the last 40 years [8]. Influential areas in control theory encompass robust control [9], time-delayed systems [10], iterative learning control [11], uncertainty quantification [12], safety-critical design [13], multi-agent systems [14], and nonlinear control [15], [16]. Moreover, theoretical guarantees for robustness and performance of feedback systems with DOs (Disturbance Observer) can be found in [16], [17], [18]. In terms of applicability, DOBC methods have proved successful implementations across a wide range of systems, including magnetic levitation systems [19], non-minimum phase pan-tilt systems [17], time-delayed wireless motion control systems [20], and multiple-input-multiple-output (MIMO) robust flight control systems both for fixed-wing [21] and quadrotor [22] examples.

While the dynamic behavior of physical systems is inherently nonlinear, the option of leveraging the Koopman operator with extended dynamic mode decomposition (EDMD) stands out as a highly effective choice for practical applications [23], including the Koopman operator-based DOBC of a mobile robot [24]. Yet, ensuring robust stability and robust performance with nonlinear representation is challenging and can be difficult to understand and implement for practitioners [25], [26], where the significance of having guaranteed margins is paramount, particularly in aerospace applications [27]. Therefore, conducting an experimental comparison, complementing existing literature reviews that may fall short in addressing practical challenges over a challenging aerospace example, becomes a guiding necessity for engineers, addressing a significant need.

Gimbal systems, recognized for their stability despite external disturbances, are designed to achieve precise target tracking and stable imaging [28], [29]. Specifically, we have selected an electro-optical gimbal system with high-performance requirements as an application example where disturbances significantly impact system performance [30]. This choice is also motivated by the growing interest in the DOBC techniques for the gimbal systems [31], [32], [33], driven by the demand for high-precision control in various fields, such as aerospace, robotics, and camera stabilization. While maintaining stability under external disturbances and uncertainties, gimbal systems face real-world performance compromises due to factors like vibrations, wind loads, and structural effects [34]. DOBC, as a promising control strategy, offers the potential to mitigate the adverse effects of disturbances, thereby enhancing the overall performance and robustness of gimbal systems. This has encouraged a growing body of research dedicated to the development and application of DOBC techniques, aiming to address the practical challenges and explore new horizons in the area of gimbal system control. The challenges brought by the gimbal system from a control theory point of view are as follows: 1) Physical features and limits of the actuators and sensors, 2) Mechanical resonances and flexible modes,

3) Stick-slip / Friction effects difficult to model, and 4) Master platform-based structural effects.

This study analyzes and compares various DOBC methods by highlighting implementation issues. Drawing inspiration from [35], the selected methods in this paper include Equivalent-Input-Disturbance (EID) [36], Uncertainty and Disturbance Estimator (UDE) [37], Active Disturbance Rejection Control (ADRC) [38], Unknown Input Observer (UIO) in Disturbance Accommodation Control (DAC) [39] and Robust Disturbance/Uncertainty Estimator (R-DUE) [17]. These methods are primarily based on linear system theory and are effective for systems with moderate disturbances and uncertainties. Recent advancements have extended DOBC applications to strongly nonlinear systems, where conventional linear methods may be insufficient. Approaches such as ADRC based on Extended State Observer (ESO) [40], nonlinear DOBC [41], and ADRC for nonlinear systems [42] address these challenges. Additionally, recent studies [43], [44], [45] provide further insights into modern DOBC techniques and applications.

To the best of our knowledge, there is no existing study that conducts a systematic and comprehensive experimental comparison of DOBC methods applied specifically to a gimbal system. Unlike previous works that focus on individual DOBC approaches, this study uniquely contributes to the field by systematically implementing and experimentally evaluating multiple DOBC methods under identical conditions. By presenting a fair comparison using performance metrics in both time and frequency domains, this work identifies practical implementation challenges, strengths, and limitations of each method. These insights aim to serve as a valuable reference for researchers and practitioners working on disturbance rejection in gimbal systems. The gimbal has also some challenging structural features, including static and dynamic imbalance, viscous friction, and a couple of resonance modes. For fairness, control systems for each DOBC method were designed with similar transient responses, inspired by their respective introductory studies, to ensure an objective comparison. Performance analysis hinges on specific criteria, including time-domain position tracking and frequency-domain disturbance rejection. Notably, all evaluated DOBC methods share the primary objective of maintaining internal and robust stability while enhancing closed-loop performance under disturbances. This shared objective establishes a solid foundation for comparing their strengths and limitations.

The problem formulation with basic assumptions is given in the following Section. In Section III, five alternative estimation methods are presented in a common framework along with their governing equations. The optimization method used to determine the parameters of the DOBC is also briefly introduced. In Section IV, dynamic behaviors of the selected DOBC methods are evaluated in both the time domain and frequency domain. Section II discusses the practical constraints and hardware in real-world applications. Finally, Section VII presents the conclusions.

II. PROBLEM FORMULATION

In this section, three different linear time-invariant (LTI) state-space representations are presented to encompass the methods used for comparison throughout this paper. In the DOBC literature, systems are typically classified based on the characteristics and influence of disturbances. Systems where disturbances act through the input channel are categorized as having matched disturbances. In contrast, when disturbances influence the system via other channels, i.e., i.e. $B_d \neq B$, they are classified as having mismatched disturbances [46]. Additionally, systems where the effects of dynamic uncertainties are aggregated and treated as disturbances are described using the concept of lumped disturbances [47]. Figure 1 illustrates the connections and distinctions among these disturbance categories. A state-space representation of a system with mismatched disturbances is provided below.

$$\begin{aligned} \dot{x}(t) &= Ax(t) + Bu_{tot}(t) + B_d d(t),\ x(0) = x_0 \\ y(t) &= Cx(t) + Du_{tot}(t) \end{aligned} \tag{1}$$

where $A \in \mathbb{R}^{n\times n}$, $B \in \mathbb{R}^n$, $C \in \mathbb{R}^{1\times n}$, $x(t) \in \mathbb{R}^n$, $u_{tot}(t) \in \mathbb{R}$, $B_d \in \mathbb{R}^{n\times n_d}$, $y(t) \in \mathbb{R}$, $d(t) \in \mathbb{R}^{n_d}$, $B \neq B_d$, and $\mathbb{R}$ denotes the set of real numbers.

If the matching condition is satisfied, meaning the disturbance acts directly through the system's input channel (i.e., $B = B_d$), the system can be represented as

$$\begin{aligned} \dot{x}(t) &= Ax(t) + B(u_{tot}(t) + d_{ed}(t)),\ x(0) = x_0 \\ y(t) &= Cx(t) + Du_{tot}(t) \end{aligned} \tag{2}$$

where $d_{ed}(t) \in \mathbb{R}$. Furthermore, assuming $x(0) = 0$ and neglecting the impact of $d_{ed}(t)$ (or $d(t)$)on the output, we obtain the corresponding transfer function (TF) representation of (2) as well as (1).

$$G(s) = C(sI - A)^{-1}B + D. \tag{3}$$

Here, I is the identity matrix, $G \in \mathbb{R}(s)$ where s denotes the Laplace operator, and $\mathbb{R}(s)$ represents the set of real rational transfer functions. While (1) and (2) can model a broad range of systems, an additional system representation is required to address *uncertainty* explicitly, thereby capturing the attitude with reduced modeling errors. The dynamics of LTI systems, accounting for *unmatched* disturbances, dynamic uncertainties, and initial conditions, can be described as [37]

$$\begin{aligned} \dot{x}(t) &= \underbrace{(A + \Delta_A)}_{\triangleq \tilde{A}} x(t) + \underbrace{(B + \Delta_B)}_{\triangleq \tilde{B}} u_{tot}(t) + d(t) \\ &\equiv Ax(t) + Bu_{tot}(t) + \underbrace{\Delta_A x(t) + \Delta_B u_{tot}(t) + d(t)}_{\triangleq d_l(t)} \\ y(t) &= Cx(t) + Du_{tot}(t),\ x(0) = x_0 \end{aligned} \tag{4}$$

where $\Delta_A \in \mathbb{R}^{n\times n}$ is the unknown yet stable system matrix, $\Delta_B \in \mathbb{R}^n$ is the unknown control matrix, and $d_l(t)$ is the lump disturbance. Similar to (3), assuming $x_0 = 0$ and neglecting $d(t)$ yield a TF for all possible plants as in [48]

$$\tilde{G}(s) \triangleq C(sI - \tilde{A})^{-1}\tilde{B} + D \equiv G(s)(1 + \Delta W_T) \tag{5}$$

where Δ denotes any stable unstructured uncertainty function satisfying $\|\Delta\|_\infty < 1$, and W_T is the robustness weight function. Now, to understand the links between (1) and (2), the following definition, adapted from [36], is useful.

Definition 1 [36]: Let the control input be $u_{tot}(t) = 0$. For disturbance $d(t)$, the output of system (1) is $y(t)$ and the output of system in (2) is $y(t)$ for disturbance $d_{ed}(t)$. The disturbance $d_{ed}(t)$ is called EID if outputs are equal, $\forall t \geq 0$.

Assumption 1: The system defined by the matrices (A, B, C) is controllable, observable, and has no poles or zeros on the imaginary axis.

Assumption 2: The system given by (2) is the minimum phase.

Assumption 3: $d(t)$ is entirely unknown but piecewise continuous and bounded.

Remark 1: Assumption 2 ensures the applicability of the comparison across all methods, as techniques like UDE and DOBC are generally not designed for non-minimum phase systems. Similarly, Assumption 3 reflects the characteristics of disturbances encountered in practical scenarios.

Remark 2: With the help of [49] and Assumption 2 for the system investigated in this paper, there always exists a bounded d_{ed} satisfying Definition 1.

Remark 3: Assumption 2 ensures the applicability of the comparison across all methods, as techniques like UDE and DOBC are generally not designed for non-minimum phase systems. Moreover, in the case of gimbal systems, which are modeled in (2) with torque disturbance as the primary exogenous input, both Assumption 2 and Assumption 3 serve as standard conditions ensuring the validity of control methodologies. Similarly, Assumption 3 reflects the characteristics of disturbances encountered in practical scenarios.

With these Remarks and Assumptions, a fair comparison can now be established. This can be achieved by scaling the disturbance across different classes of system representations to ensure an equivalent effect on the system states.

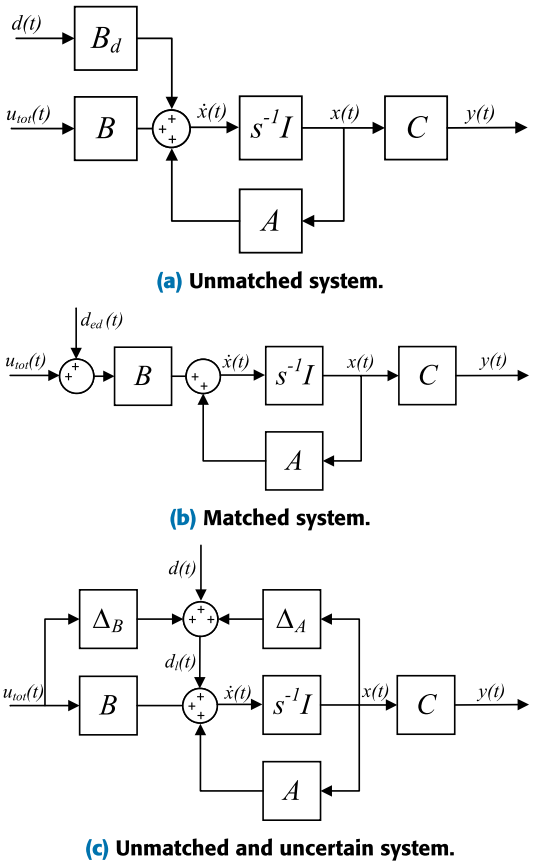

FIGURE 1. State space representations considered under the assumption of $D = 0$.

III. DISTURBANCE OBSERVER BASED CONTROL METHODS

A. FREQUENCY DOMAIN DISTURBANCE OBSERVER BASED DESIGN

One of the first studies, focusing on the estimation and cancellation of external disturbances, was introduced by Ohishi [6], where all dynamic outcomes, except for the *nominal behavior*, are treated as *lumped disturbance*. [6] and the following methods attempted to reject these *lumped disturbances* using nominal inverse dynamics, showcasing a strong relation with *stable inversion*. Dynamic inversion, and consequently, the consideration of only minimum phase systems, posed limitations in these early studies. Although some modifications have been proposed to extend the method to non-minimum phase systems [50], [51], the fundamental concept predominantly revolves around *stable inversion* with an initial emphasis on minimum phase systems.

The block diagram of the original work is given in Figure 2. Here $C(s)$ represents the main control system, $\tilde{G}(s)$ denotes the real system, $G(s)$ is the nominal system choice, and $Q(s)$ stands for the Q-filter that a detail discussion will be given. The lumped disturbance d_l is obtained through the inverse of the nominal plant and is implementable solely for *proper* nominal system choices. To generalize the method and have some flexibilities under noise attenuation, the Q-filter must be considered where the output is the estimation of disturbance $\hat{d}$.

The transfer function representation from the input $u(t)$ to the output $y(t)$ is given in (3).

The generalized expression of a high-order transfer function is as follows.

$$G(s) \triangleq \left\{ \frac{\sum_{i=1}^{m} b_i s^i}{\sum_{i=1}^{n} a_i s^i} \right\} \quad k \triangleq n - m \tag{6}$$

where k is the relative degree.

The following are utilized to get the analytical forms of lump disturbance and its estimation.

$$\begin{aligned} d_l(s) &= d_{ed}(s) - G(s)^{-1} n(s) + [G(s)^{-1} - \tilde{G}(s)^{-1}] y(s) \\ \hat{d}(s) &= d_l(s) Q(s) \end{aligned} \tag{7}$$

where $d_{ed}(s) \triangleq \mathcal{L}\{d_{ed}(t)\}$, $y(s) \triangleq \mathcal{L}\{y(t)\}$, and $n(s) \triangleq \mathcal{L}\{n(t)\}$. Here $\mathcal{L}\{\cdot\}$ is the Laplace transform.

Remark 4: Note that, with respect to (1)-(2), we can always find inverses of $G(s)$ and $\tilde{G}(s)$ in (7). However, for the

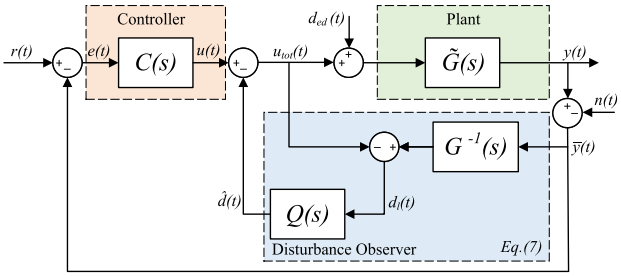

FIGURE 2. Disturbance obverser based control structure [35].

cases where inverses do not exist one can use the algebraic methods introduced in [49].

In (7), every factor that deviates from the nominal behavior can be regarded as a lump disturbance. The potential sources in d_l (as in $\hat{d}$) encompass modeling errors in $G(s)$ (i.e., neglected nonlinear dynamics, parameter variations), measurement noise, and external disturbances where the design of $Q(s)$ plays a pivotal role since the $\hat{d}(s)$ is directly used in the feedback structure ($\hat{d}(s) = d_l(s)Q(s)$).

1) ON THE DESIGN OF Q-FILTER $Q(S)$

The significance of the Q-filter in a disturbance-observer-based control (DOBC) structure is crucial for both disturbance estimation performance and the system's stability, as highlighted in [52]. Various studies, including [53], [54], and [55], explore modifications to the Q-filter to enhance DOBC performance. Additionally, design guidelines are offered in works such as [56] and [57], contributing valuable insights into design and implementation issues of the Q-filter for improved disturbance estimation and compensation. While the Q-filter is typically viewed as a low-pass filter in most studies, exploring alternative structures offers insights into the underlying mechanisms of disturbance estimation. Influenced by [17], this section aims to elucidate the relationship between estimation performance and the Q-filter, offering a comprehensive guideline supported by an illustrative example.

The main aims of the Q-filter are twofold:

1) Establishing a DO part, characterized by a simple inverted dynamics that is either proper or strictly proper, ensures an implementable and feasible DO structure.
2) Determining and defining the performance bounds for disturbance estimation at each frequency.

For instance, for a perfect disturbance estimation in magnitude, $|Q(j\omega)| \approx 1 \quad \forall\omega$. In this case, perfect magnitude estimation (neglecting phase lag for simplicity) yields an all-pass filter as a Q-filter. However, challenges associated with selecting an all-pass filter as the Q-filter include:

1) Sensitivity to measurement noises, and
2) An improper disturbance observer part where $k \neq 0$ in (6).

Moreover, to estimate the disturbance's components within a specific frequency range as

$$Q(j\omega) \triangleq \begin{cases} |Q(j\omega)| \approx 1 & \forall\omega \in [\omega_1, \omega_2] \\ |Q(j\omega)| \approx 0 & \forall\omega \notin [\omega_1, \omega_2] \end{cases} \tag{8}$$

a band-pass filter should be utilized.

Example 1: A swept sine, also known as a "periodic chirp", refers to a sine sweep test wherein the frequency ascends or descends within a single measurement period, and this process repeats to generate a periodic signal [58]. Frequency is swept ascending linearly as given in (9).

$$\begin{aligned} d(t) &= A\sin(2\pi f_i(t)t + \phi), \quad 0 \le t \le T_0 \\ f_i(t) &= f_{start} + \beta t, \quad \beta = (f_{end} - f_{start})/T_0 \end{aligned} \tag{9}$$

where T_0 is the signal period and ϕ is the initial phase. f_{start} and f_{end} are the lowest and highest frequencies of interest, respectively.

The Q-Filter, which should be strictly proper and stable, can be in the low-pass, band-pass, or all-pass transfer function forms. Their expressions are as follows:

Low Pass Filter Design:

$$Q(s) = \frac{1}{(T_q s + 1)^k}, \quad \omega_c = \frac{1}{T_q} \tag{10}$$

where ω_c is the cutoff frequency of the low-pass filter. It represents the bandwidth for DO.

Band Pass Filter Design:

$$Q(s) = \frac{(\omega_c/Q_f)s}{s^2 + (\omega_c/Q_f)s + {\omega_c}^2} \tag{11}$$

where ω_c is the center frequency of the passband filter. Also, Q_f is the filter's quality factor, determining the bandwidth.

All Pass Filter Design:

$$Q(s) = \frac{s - \omega_0}{s + \omega_0} \tag{12}$$

where ω_0 is the corner frequency of the all-pass filter. To use an all-pass filter, the relative degree of the representation of the system expressed in (6) must be 0.

Let's consider a system, as depicted in Figure 2, that is proper, minimum-phase, stable, and $k = 0$ in (6). Additionally, $n(t) = 0$ has been considered.

$$\tilde{G}(s) = \frac{s + 10}{s + 2}, \quad G^{-1}(s) = \frac{s + 2}{s + 10} \tag{13}$$

In the equation defined in (9) and utilized as the disturbance signal in this example, $T_0 = 2$, $\phi = 0$, $f_{start} = 1$ Hz, and $f_{end} = 50$ Hz are chosen. In (10), $\omega_c = 2\cdot\pi\cdot 20$ and $k = 1$ are chosen; in (11), $\omega_c = 2\cdot\pi\cdot 20$ and $Q_f = 1$ are chosen; and in (12), $\omega_0 = 1$ is chosen.

Let's substitute (13) into the structure given in Figure 2. In the DOBC structure designed with the selected parameters, the time-domain responses of the estimated disturbances obtained after chirp disturbance and different Q-Filter structures are presented in Figure 3. Furthermore, the frequency domain responses calculated using the Fast Fourier

Transform (FFT) are also provided in Figure 4. To enhance the clarity of the LPF, BPF, and APFs, time-dependent boundary envelopes have been incorporated into Figure 3. These envelopes are also observed in the frequency spectrum of the estimated disturbance shown in Figure 4.

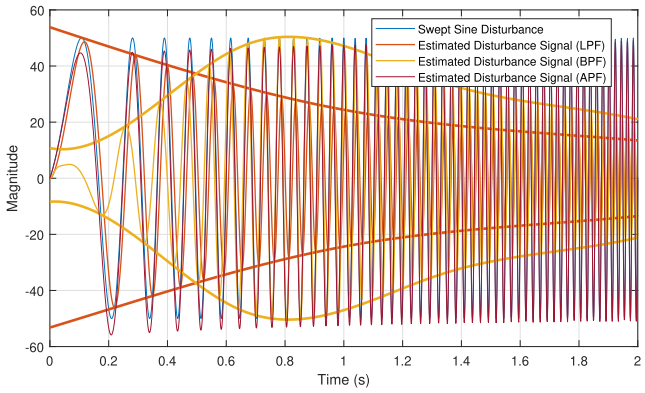

FIGURE 3. Disturbance swept sine time domain.

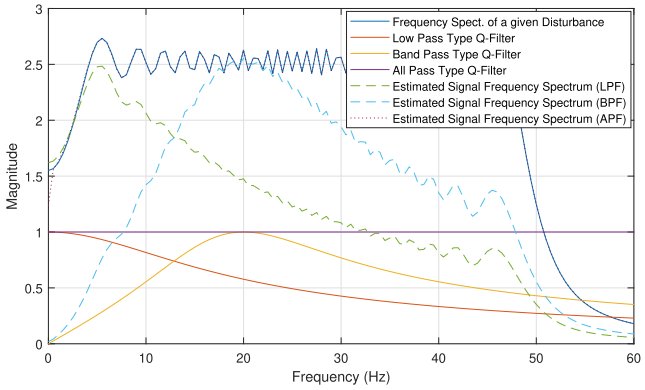

FIGURE 4. Disturbance swept sine frequency domain.

2) ON THE DESIGN OF CONTROLLER C(S)

The recommended method for C(s) design is state feedback control. The control input,

$$u_{tot}(t) = \underbrace{(-Kx(t))}_{u(t)} - \hat{d}(t) \tag{14}$$

$$C(s) = \frac{U(s)}{E(s)} = \frac{-KX(s)}{R(s) - CX(s)} \tag{15}$$

can be calculated.

B. UNKNOWN INPUT OBSERVER IN DISTURBANCE ACCOMMODATION CONTROL

Unknown Input Observer (UIO) in [39], introduced by Johnson in the late 1960s, is a powerful method in DOBC. Ohnishi's method and Johnson's approach complement each other, similar to how frequency domain methods complement modern control methods.

Disturbance Accommodation Control (DAC) is an effective control method developed to enhance the robustness of systems against external disturbances. Particularly in systems with incomplete or partial state information, the UIO structure enhances the effectiveness of the DAC approach by providing both state estimation and disturbance estimation. This paper examines the role of UIO within the DAC framework, covering its theoretical foundations and practical implementation steps.

The UIO jointly estimates both system states and disturbance if system states are unavailable. Consider (2) define

$$\begin{aligned} \dot{\xi}(t) &= W\xi(t) \\ d_{ed}(t) &= V\xi(t) \end{aligned} \tag{16}$$

where W and V are presumed known matrices.

The state observer equation is given in (17)

$$\begin{aligned} \dot{\hat{x}}(t) &= A\hat{x}(t) + B(u(t) + \hat{d}(t)) + L_x\left(y(t) - \hat{y}(t)\right) \\ \hat{y}(t) &= C\hat{x}(t) \end{aligned} \tag{17}$$

where $\hat{x}$ and $\hat{d}$ are the estimated states and disturbance. L_x is the state observer gain.

The disturbance observer equation is given in (18)

$$\begin{aligned} \dot{\hat{\xi}}(t) &= W\hat{\xi}(t) + L_d\left(y(t) - \hat{y}(t)\right) \\ \hat{d}(t) &= V\hat{\xi}(t) \end{aligned} \tag{18}$$

where $\hat{\xi}$ is the estimate of ξ and L_d is the disturbance observer gain.

In Equation (2), the effective control signal $u_{tot}(t)$ is obtained by subtracting the estimated disturbance $\hat{d}(t)$ from the main controller's control signal $u(t)$.

$$u_{tot}(t) = u(t) - \hat{d}(t) \tag{19}$$

Figure 5 presents a block diagram representation of the combined form of the equations given in (2), (16), (17), (18), and (19).

C. UNCERTAINTY AND DISTURBANCE ESTIMATOR

UDE-based control [59], described in this section, incorporates three key components: the reference model, the filter, and the error feedback gain. This method effectively estimates the combined effects of uncertainty and disturbance.

Consider a stable closed-loop reference system dynamics as

$$\dot{x}_m(t) = A_m x_m(t) + B_m r(t) \tag{20}$$

where $A_m \in \mathbb{R}^{n\times n}$, $B_m \in \mathbb{R}^n$, $x_m(t) \in \mathbb{R}^n$, $r(t) \in \mathbb{R}$ is the desired or reference state.

Then, for UDE, (4) is simplified by grouping the uncertainty and disturbance terms into a single lumped disturbance, expressed as:

$$\dot{x}(t) = (A + \Delta_A)x(t) + (B + \Delta_B)u_{tot}(t) + d(t) \tag{21}$$

$$= Ax(t) + Bu_{tot}(t) + d_l(t) \tag{22}$$

$$\therefore \quad d_l(t) = \dot{x}(t) - Ax(t) - Bu_{tot}(t) \tag{23}$$

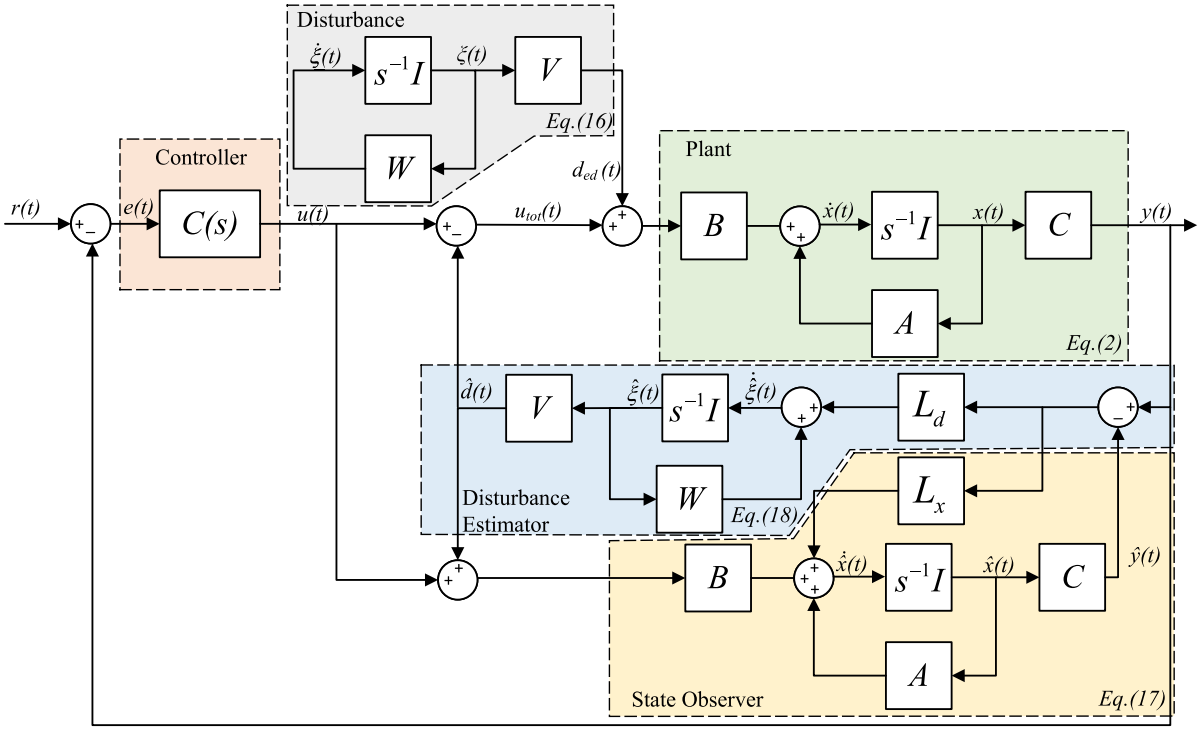

FIGURE 5. Unknown input observer in disturbance accommodation control structure.

The goal of UDE is to design a control input $u_{tot}(t)$ such that the system state $x(t)$ in (21) asymptotically tracks the reference state $x_m(t)$ in (20). This requires ensuring that the tracking error:

$$e(t) \triangleq x_m(t) - x(t) \in \mathbb{R}^n \tag{24}$$

satisfies:

$$\lim_{t\to\infty} (x_m(t) - x(t)) = 0 \tag{25}$$

and thus

$$\dot{e}(t) = (A_m + K_e)\, e(t) \tag{26}$$

where $K_e \in \mathbb{R}^{n\times n}$ is the error feedback gain matrix, and $(A_m + K_e)$ is Hurwitz [60]. Several design strategies for K_e are available such as setting $K_e = 0$ or using pole placement methods [59], [61]. The primary aim is to reduce the high-frequency components of the uncertainty and disturbance signal [37]. Using (24), we can rewrite (26) and then expanding it and solving for u_{tot} yields

$$\begin{aligned}
&\Big(\overbrace{A_m x_m(t) + B_m r(t)}^{\dot{x}_m(t)} \\
&\underbrace{-Ax(t) - Bu_{tot}(t) - d_l(t)}_{-\dot{x}(t)}\Big) = \underbrace{A_m x_m(t) - A_m x(t)}_{A_m e(t)} + K_e e(t) \\
&Bu_{tot}(t) = A_m x(t) + B_m r(t) - Ax(t) - d_l(t) - K_e e(t) \\
&u_{tot}(t) = B^{\dagger}\big[A_m x(t) + B_m r(t) - Ax(t) - d_l(t) - K_e e(t)\big]
\end{aligned} \tag{27}$$

where $B^{\dagger} \triangleq (B^T B)^{-1} B^T$, such that $B^{\dagger}B = I$ is called as pseudo-inverse and always exists for SISO systems. However, the perfect control input u_{tot} is not directly applicable, as calculating $d_l(t)$ in (27) requires pure differentiation of $\dot{x}(t)$, as shown in (23). To address this challenge, the UDE design procedure (see [59]) proposes using an approximation of $d_l(t)$, expressed as

$$\hat{d}(t) = d_l(t) * q(t) \tag{28}$$

$$= (\dot{x}(t) - Ax(t) - Bu_{tot}) * q(t). \tag{29}$$

where the "$*$" operator is the convolution operation and $q(t) \triangleq \mathcal{L}^{-1}\{Q(s)\}$. To get the original form of the UDE, we replace (29) in (27),

$$\begin{aligned}
u_{tot}(t) = -B^{\dagger}\Big(&Ax(t) - A_m x(t) - B_m r(t) + \\
&(\dot{x}(t) - Ax(t) - Bu_{tot}(t)) * q(t) + K_e e(t)\Big)
\end{aligned} \tag{30}$$

and take the Laplace transform as

$$\begin{aligned}
U_{tot}(s) &= -B^{\dagger} + \Big(AX(s) - A_m X(s) - B_m R(s) \\
&\quad + \big(sX(s) - AX(s) - BU_{tot}(s)\big)Q(s) + K_e E(s)\Big) \\
&= -B^{\dagger}\Big(AX(s) - \frac{sQ(s)}{1-Q(s)}X(s) \\
&\quad - \frac{1}{1-Q(s)}A_m X(s) + B_m R(s) - K_e E(s)\Big)
\end{aligned} \tag{31}$$

and by taking the inverse Laplace transformation, we get the applicable UDE-based control.

$$u_{tot}(t) = -B^{\dagger}\left(Ax(t) + \mathcal{L}^{-1}\left\{\frac{sQ(s)}{1-Q(s)}\right\} * x(t) - \mathcal{L}^{-1}\left\{\frac{1}{1-Q(s)}\right\} * \left(A_m x(t) + B_m r(t) - K_e e(t)\right)\right) \quad (32)$$

The implementation of (32) can be represented by the block diagram in Figure 6. A critical component of this framework is the Q-filter, which shapes the estimation of the lumped disturbance $d_l(t)$. In designing $Q(s)$, the methods described in Section III can be utilized. A common choice for $Q(s)$ is a low-pass filter with the appropriate form, as given in (10).

Additionally, to isolate $\hat{d}(t)$ from the control input, or equivalently, to disable the uncertainty and disturbance estimation in (32), we can set $Q(s) = 0$, which implies $q(t) = 0$ and consequently:

$$d_l(t) * q(t) = d_l(t) * 0 = 0 \quad \Longrightarrow \quad \hat{d}(t) = 0.$$

While UDE offers advantages such as its low-order form and design simplicity, requiring adjustment of only three parameters, there are limitations to its applicability. Notably, UDE is not suitable for time-delayed or non-minimum phase systems, and it relies on full-state measurement, which may be impractical in certain industrial applications. For detailed discussions on these limitations and potential solutions, see [62] and [63].

D. EQUIVALENT INPUT DISTURBANCE ESTIMATOR

In this section, EID [36] is introduced as another modern control-based method to estimate and compensate for lumped disturbances. The block diagram of the EID-based control method is shown in Figure 7.

For the state observer

$$\dot{\hat{x}}(t) = A\hat{x}(t) + Bu(t) + L\left(y(t) - C\hat{x}(t)\right) \quad (33)$$

is expressed with. Here, L is the observer gain, and its design is made with LQR, which is an optimal control method.

Let the difference between the estimated state and the system state be

$$\delta x(t) = \hat{x}(t) - x(t) \quad (34)$$

Without loss of generality, we can assume $\tilde{A} = A, \tilde{B} = B$, then substituting (34) into (2) gives

$$\dot{\hat{x}}(t) = A\hat{x}(t) + Bu_{tot}(t) + \{Bd_{ed}(t) + [\delta\dot{x}(t) - A\delta x(t)]\} \quad (35)$$

Differences between state estimation and the actual state also affect disturbance estimation. Suppose there is a $\delta d(t)$ control input that satisfies

$$\delta\dot{x}(t) - A\delta x(t) = B\delta d(t) \quad (36)$$

When the equation (36) is substituted in (35) and placed in the common parenthesis B, (37) is obtained.

$$\dot{\hat{x}}(t) = A\hat{x}(t) + B(u_{tot}(t) + [d_{ed}(t) + \delta d(t)]) \quad (37)$$

The lump disturbances estimated by the EID is expressed by (38).

$$d_l(t) = d_{ed}(t) + \delta d(t) \quad (38)$$

It allows us to express the system as follows.

$$\dot{\hat{x}}(t) = A\hat{x}(t) + B[u_{tot}(t) + d_l(t)] \quad (39)$$

If the right-hand sides of (33) and (39) are equalized, we get (40).

$$B[d_l(t) + u_{tot}(t) - u(t)] = LC[x(t) - \hat{x}(t)] \quad (40)$$

and solving for $d_l(t)$ and applying Q-filter yields

$$d_l(t) = B^{\dagger}LC\left[x(t) - \hat{x}(t)\right] + u(t) - u_{tot}(t) \quad (41)$$

$$\hat{d}(t) = d_l(t) * \mathcal{L}^{-1}\{Q(s)\}$$

$$\hat{D}(s) = D_l(s)Q(s) \quad (42)$$

$D_l(s)$ and $\hat{D}(s)$ are Laplace transforms of $d_l(t)$ and $\hat{d}(t)$, respectively. $\hat{d}(t)$ is the resulting disturbances estimate. In addition, $Q(s)$ represents a low-pass filter in the form of (10) that determines the bandwidth of the disturbance estimator. Finally, the effective control signal is given by $u_{tot}(t) = u(t) - \hat{d}(t)$. The proposed block diagram structure for the EID structure is given in Figure 7.

First, a single augmented-state representation (43) is constructed with the disturbances neglected step signal and an internal model of the system [36]. A_R and B_R represent the internal model parameters (the step is the model used to improve the input vs. tracking performance) in the control system.

$$\begin{bmatrix}\delta\dot{x}(t)\\ \delta\dot{x}_R(t)\end{bmatrix} = \begin{bmatrix}A & 0\\ -B_RC & A_R\end{bmatrix}\begin{bmatrix}\delta x(t)\\ \delta x_R(t)\end{bmatrix} + \begin{bmatrix}B\\ 0\end{bmatrix}\delta u(t) \quad (43)$$

where $\delta x(t) = x(t) - x(\infty)$, $\delta x_R(t) = x_R(t) - x_R(\infty)$, and $\delta u(t) = u(t) - u(\infty)$

K_P and K_R in Figure 7 are state feedback gains and are calculated by the linear quadratic regulator (LQR) (44).

$$J_K = \int_0^{\infty}\left\{[\delta x^T(t)\delta x_R^T(t)]Q_K\begin{bmatrix}\delta x(t)\\ \delta x_R(t)\end{bmatrix} + R_K\delta u^2(t)\right\}dt \quad (44)$$

L represents the observer gain and is calculated similarly to the LQR (45).

$$J_L = \int_0^{\infty}\{\rho x_L^T(t)Q_L x_L(t) + R_L u_L^2(t)\}\,dt \quad (45)$$

E. DISTURBANCE/UNCERTAINTY ESTIMATOR BASED ROBUST CONTROL

This method, the disturbances estimate, and the main control system are not handled separately; instead, two $\mathcal{H}_\infty$ syntheses are handled as a whole to ensure robust stability and performance. The proposed block diagram structure for the DUEBRC structure is given in Figure 8. Here, $C(s)\mathcal{H}_\infty$ designed the main control system, $\tilde{G}(s)$ the real system to be controlled, $G(s)$ control syntheses and the nominal system model used in the method, $C_{obs}(s)$ represents the control

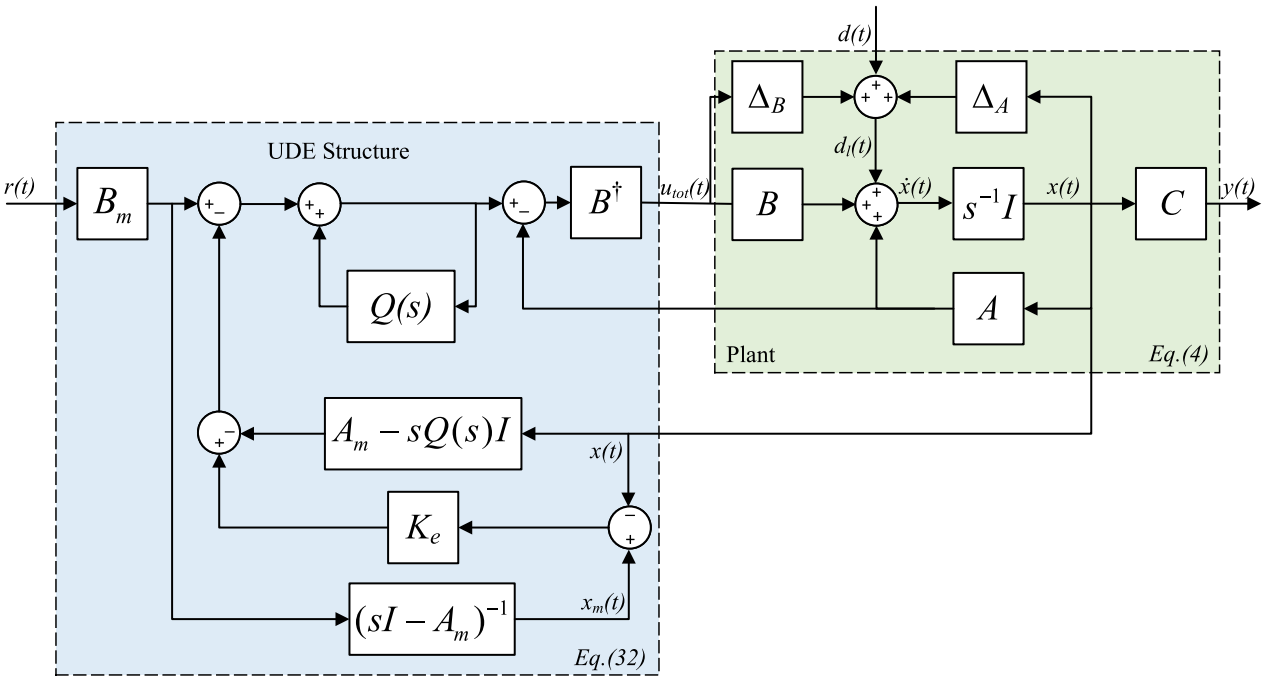

FIGURE 6. Uncertainty and disturbance estimator structure.

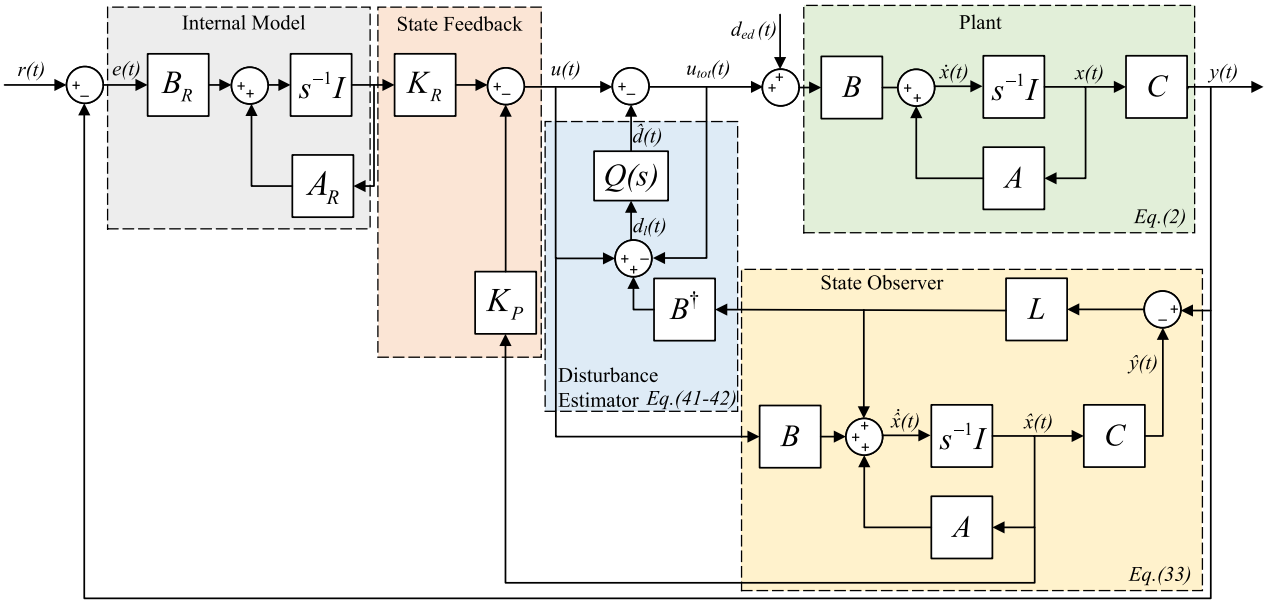

FIGURE 7. Equivalent input disturbance structure.

system of the disturbance-observer loop designed with $\mathcal{H}_\infty$ and $\hat{d}$ represents the disturbances estimate obtained as a result of the method. The integrated control system design is given below, step by step.

- Determine the frequency range of the d_{ed} disturbance that is desired to be suppressed

$$\hat{d}(j\omega) = d_{ed}(j\omega) \mid \forall\omega \in (0, \omega_r]. \tag{46}$$

Here, ω_r denotes the upper limit of the frequency components for which suppression of disturbances is desired.

- With the provision of (46) and the support of Figure 8

$$\begin{aligned}\varepsilon(j\omega) &= (1 + G(j\omega)C_{obs}(j\omega))^{-1}(y - \hat{y}) \\ &= S_{obs}(j\omega)(y - \hat{y})\end{aligned}$$

$$= (1 - T_{obs}(j\omega))(y - \hat{y})$$
$$\approx 0 \mid \forall\omega \in (0, \omega_r] \tag{47}$$

The design of C_{obs} is required to ensure the equation. It should be noted that this design should be made on the nominal system and that no uncertainty should be added to the design.

- After designing the control system of the disturbance observer loop, the robustness weight matrix W_T to be used in the design of the main control system will be updated according to Corollary 1 of [17], taking into account S_{obs} and T_{obs}. $C(s)$ will be designed according to the weight matrix.

The reader can refer to [17] for design details.

The aim is to obtain clear mathematical expressions for robust stability, performance, and bandwidth requirements in disturbance/uncertainty estimator-based control. The structure obtained as a result of the design guarantees robust stability and performance analytically.

IV. DESIGN AND ANALYSIS

Inertially stabilized platforms, known as EO/IR (Electro-Optical/Infra-Red) gimbals, aim to provide a stable line of sight for tracking stationary and dynamic targets. These are utilized in applications ranging from photography and videography, for camera stabilization, to advanced aerospace technologies. The rotational motion of gimbal axes is facilitated by various electrical actuators, such as servo, stepper, and even piezo or voice coil motors. For precise positioning, they operate in a closed-loop system with some measurement devices (i.e., a high-resolution rotary encoder, and IMU (Inertial Measurement Unit)) on each axis. Analyzing the 2-axis stability presents a complex challenge. This emphasizes the need for advanced controllers, specifically designed for evaluating and enhancing performance limits under uncertain conditions.

A gimbal system with high complexity and high-performance requirements was chosen for a meaningful comparison of the abovementioned methods and explained in detail. Although it is possible to expand MIMO with a certain effort, only one axis of the gimbal system is considered a SISO system to increase intelligibility and repeatability. The outer axis is called the azimuth axis, and the inner axis is called the elevation axis. In this study, the input of the system model of interest is the torque applied from the motor on the elevation axis, and its output is the angular velocity read from the gyroscope of the IMU.

The transfer function of the system is expressed as follows:

$$G(s) = G_{TSD}(s)G_{RBD}(s)$$
$$G_{RBD}(s) = \frac{1}{Js + b}$$
$$G_{TSD}(s) = G_r(s)G_{ar}(s)$$
$$G_r(s) = \prod_{i=1}^{r} \frac{s^2 + \omega_{w_i}s + \omega_{c_i}^2}{s^2 + (\omega_{w_i}/m_i)s + \omega_{c_i}^2}$$
$$G_{ar}(s) = \prod_{i=1}^{ar} \frac{s^2 + (\omega_{w_i}/m_i)s + \omega_{c_i}^2}{s^2 + \omega_{w_i}s + \omega_{c_i}^2} \tag{48}$$

where $G_{TSD}(s)$ is torsional structural dynamic transfer function, $G_{RBD}(s)$ is rigid body dynamic transfer function, $G_r(s)$ and $G_{ar}(s)$ are torsional resonances and torsional anti-resonances terms of $G_{TSD}(s)$, respectively. The torsional resonance and anti-resonance dynamics are characterized by the cutoff frequency ω_c, width ω_w, and magnitude m.

There are various techniques for modeling a two-axis gimbal. The entire dynamic model, including their cross-coupling effects, can be modeled using Abdo et al.'s model [64], and then the control design can be initiated. Alternatively, the system can be modeled through system identification based on input-output datasets [65]. As done in this study, the modeling can be approached by dividing it into two parts: rigid body dynamics and torsional structural dynamics. The model can be validated using Frequency Response Function (FRF) results.

This system is represented as a state space by (2).

$$A = \begin{bmatrix} -663.2 & -1358 & -358.2 & -851.1 & -37.23 \\ 2048 & 0 & 0 & 0 & 0 \\ 0 & 1024 & 0 & 0 & 0 \\ 0 & 0 & 1024 & 0 & 0 \\ 0 & 0 & 0 & 32 & 0 \end{bmatrix}$$
$$B = \begin{bmatrix} 64 & 0 & 0 & 0 & 0 \end{bmatrix}^T$$
$$C = \begin{bmatrix} 2.119 & 0.5634 & 2.81 & 0.8684 & 56.33 \end{bmatrix} \quad D = 0$$

The system with transfer function representation (3) is stable and has a minimum phase.

When the mathematical model of the system is obtained through calculations based on the known dynamics of the system, as seen in Figure 9, the model is consistent and rational. Additionally, the advantages of using the recommended modeling technique instead of the system identification toolbox are as follows:

1) System identification may not always be possible or it may require a significant amount of accessible data.
2) It is possible that some dynamics may not be clearly understood or even captured by system identification techniques.

When the mechanical structures driven from one side are not symmetrical, resonance is expected at some frequencies due to the torsional effect. In addition, the first mode frequency is found from the relationship between the gimbal payload inertia moment and the rotor inertia moment of the motor, the equivalent inertial moment value, and the rotational spring coefficient. For more detailed information on the subject, readers can review the article written by Kristin Lewotsky [66]. It is possible to eliminate this mode frequency in the system model, move it further, or reduce its amplitude by changing the mechanical structure and motor layout. However, for systems that cannot be changed in the system model, it is necessary not to stimulate the mode frequency with the torque to be applied from the motor part.

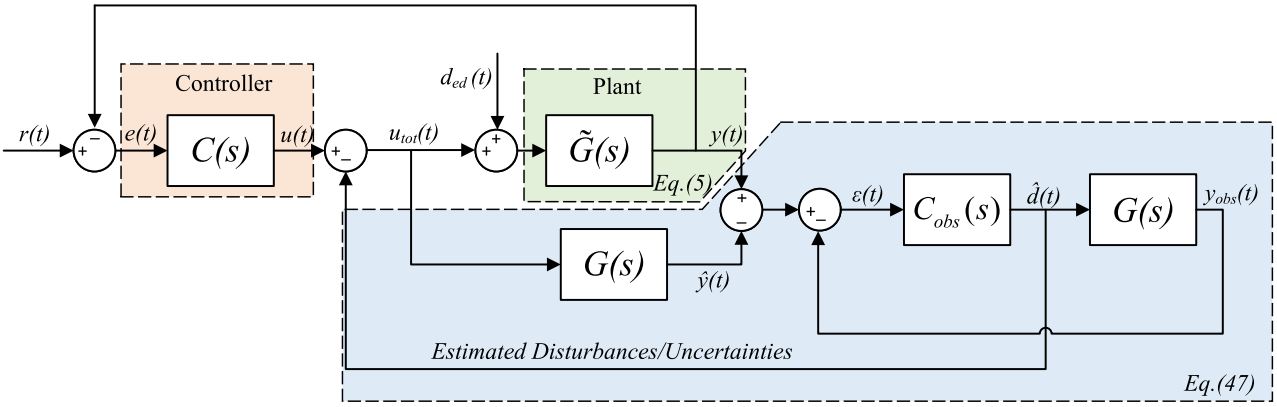

FIGURE 8. Disturbance/Uncertainty estimator based robust control block diagram.

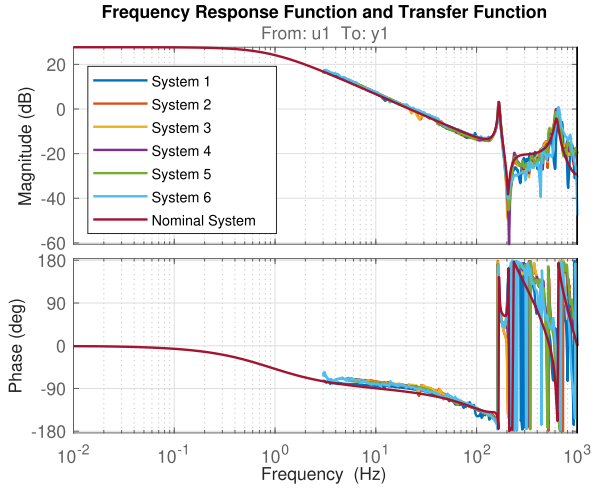

(a) Frequency response function (FRF) and nominal transfer function.

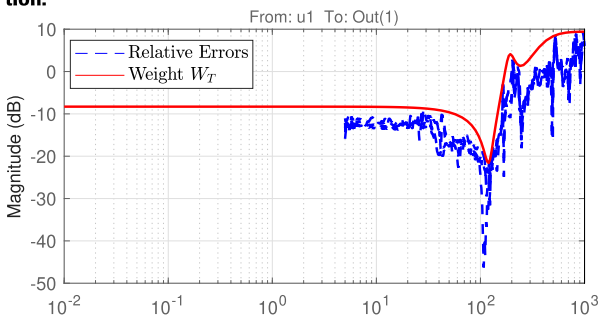

(b) Relative errors for experimental data, a high order bounding weight W_T.

FIGURE 9. The system identification from the experimental dataset.

The most primitive solution is to design a notch filter for the output of the control signal.

A. FREQUENCY DOMAIN DISTURBANCE OBSERVER BASED DESIGN

This structure achieves the design with a state feedback controller method. All the states of the system are used over the nominal plant. While finding the state feedback gains, the gain coefficients that minimize the settling time were found with the gradient descent algorithm. An additional one is multiplied by a gain over the error state. Since the number of poles of the system model is one more than the number of zeros, the inverse of the plant is multiplied by $w_c = 251$ rad/s, a low pass filter (10) to make it proper. The control input signal is also passed through the same low-pass filter (10), and the difference between them enters the system's main controller with a negative signal as an estimated disturbance. At the same time, this estimated disturbance signal is collected with the control signal before the input of the nominal plant.

In the gradient descent algorithm, state feedback gains are initially assigned to ensure system stability. The coefficients were then iteratively updated until the gradient became positive. Iterations continued until the gradient was positive four times. Among these iterations, the coefficient that minimizes the settling time, representing the smallest local minimum, was determined. To refine this process, the gradient descent algorithm was applied separately to each coefficient, and at each step, the coefficient yielding the smallest cost function was retained, as shown in Figure 10. The state feedback gain coefficients obtained as a result of the optimization are as follows:

$$K = [5.012 \;\; 19.982 \;\; 10.168 \;\; 10.138 \;\; 41.901 \;\; -31.313].$$

B. UNKNOWN INPUT OBSERVER IN DISTURBANCE ACCOMMODATION CONTROL

In Johnson's article [39], a design was made with the conventional optimal linear regulator theory. In the main controller design phase of this study, since all methods are compared to the step response without disturbance, it was designed with LQI so that there is no steady-state error. Similar to the previous section, the initial values of the weighting matrix Q and R were chosen to make the state feedback gains system stable due to the optimization. In each iteration, the Riccati equation is solved, and as a result,

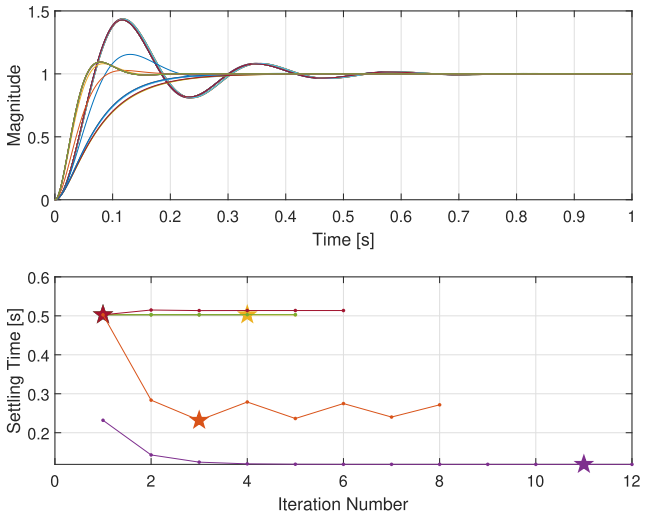

FIGURE 10. Settling time and step responses according to iterations.

the diagonal elements of the Q and R matrices are updated according to the settling time criterion. In the Observer design, there are 4 gain parameters W, V, L_x, and L_d. Parameters that minimize the error between the disturbance signal and the estimated disturbance signal have been found. The state feedback gain coefficients obtained as a result of the optimization are as follows:

$$K = [16.022 \quad 8.826 \quad 14.468 \quad 2.383 \quad 40.711 \quad -29.074].$$
$$V = 2.3125, \quad W = 9.9903, \quad L_x = 100, \quad L_d = 200$$

Step response graphics and settling time values obtained when state feedback gains, which are updated according to iterations, are substituted, are given in Figure 11.

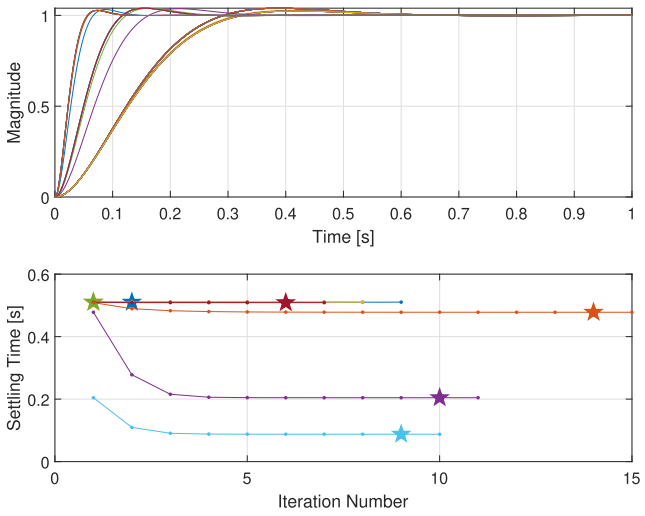

FIGURE 11. Settling time and step responses according to iterations.

C. UNCERTAINTY AND DISTURBANCE ESTIMATOR

In this structure, no feedback is received from the system output. The error feedback gain is multiplied by the difference between the system states and the states of the reference model. Therefore, both the reference model and the system model have been converted to observable canonical form. If it is not done in this way, a steady-state error occurs. In this system structure, the reference model for UDE has been chosen to be close to the system response of other methods, whose gradient descent and controller parameters are calculated. Reference model, with $\omega_n = 160$ and $\zeta = 0.65$, is a second-order transfer function.

$$G_m(s) = \frac{\omega_n^2}{s^2 + 2\zeta\omega_n s + \omega_n^2} G_{res}$$

where G_{res} is the residual stable transfer function with non-dominant system poles and zeros and $(m-2)$ order, m is the order of the system. Non-dominant poles are placed further away from dominant poles to minimize their influence on system dynamics and ensure predictable control behavior [67].

The error feedback gain K_e is chosen to be 0. The low-pass filter also has the same bandwidth as in all methods.

D. EQUIVALENT INPUT DISTURBANCE ESTIMATOR

In the article of She et al. [36], the main controller was designed with an optimal control method. Since there is a similar design in the (UIO in DAC) method, the state feedback gains (K_P and K_R) designed in that part are used. The low-pass filter also has the same bandwidth as in all methods. The A_R and B_R coefficients were chosen as 0 and 1, respectively. First, the disturbance was neglected and a single augmented state representation (43) was created, which included an internal model of the step signal and the plant.

The Q_K and R_K values for which the minimum settling time value is reached as a result of the optimization are as follows:

$$Q_K = \text{diag}[1\ 1\ 1\ 1\ 7.51\ 38.51], \quad R_K = 0.0455$$

yields

$$K_P = [16.02209 \quad 8.82660 \quad 14.4689 \quad 2.3830 \quad 40.7110].$$
$$K_R = -29.07437$$

The results obtained in Figure 11 are quite close to those obtained with the EID structure.

$$Q_L = \text{diag}[2 \quad 2 \quad 2 \quad 2 \quad 2], \quad R_L = 0.5$$
$$L = [629.729 \quad 411.372 \quad 268.75 \quad 87.59 \quad 28.536]^T$$

E. DISTURBANCE/UNCERTAINTY ESTIMATOR BASED ROBUST CONTROL

With the weighted mixed-sensitivity $\mathcal{H}_\infty$, both the main controller and the observer controller are designed. In this design, it is theoretically possible to increase the sensitivity weighting filter bandwidth without any control input limitation. The optimization method has been implemented as an LMI-based algorithm.

The sensitivity weighting filter is given in (49).

$$W_P(s) = \left(\frac{s/\sqrt[\kappa]{M_P} + \omega_P}{s + \omega_P \sqrt[\kappa]{\xi_P}}\right)^{\kappa} \tag{49}$$

The control weighting filter is given in (50).

$$W_U(s) = \left(\frac{s + \omega_U/\sqrt[\kappa]{M_U}}{s\sqrt[\kappa]{\xi_U} + \omega_U}\right)^{\kappa} \tag{50}$$

The uncertainty weighting filter is given in (51).

$$W_T(s) = \left(\frac{s + \omega_T/\sqrt[\kappa]{M_T}}{s\sqrt[\kappa]{\xi_T} + \omega_T}\right)^{\kappa} \tag{51}$$

Both the observer part and the main controller weighting filter parameters are provided in Table 1.

TABLE 1. All weighting filter parameters.

Weighting Filters	M	ω	κ	ξ
W_P	1.05	$2\ \pi\ 5$	1	10^{-5}
W_U	N/A	N/A	N/A	N/A
W_T	1.25	$2\pi 20$	1	0.667
$W_{P_{obs}}$	1	$2\pi 50$	1	10^{-5}
$W_{U_{obs}}$	10^4	N/A	1	10^4
$W_{T_{obs}}$	N/A	N/A	N/A	N/A

F. OPTIMIZATION AND PERFORMANCE CRITERION

In this publication, the gradient descent method has been used to determine the parameters of the main controllers, as explained in the pioneering studies of the estimator-based control methods. Gradient descent is an optimization approach for minimizing the error function and settling time derived from time-domain responses.

$$K_{i+1} = K_i - \eta \frac{\partial}{\partial K_i} J(K_i, x, u, t) \tag{52}$$

In this algorithm, the objective function is updated iteratively for the number of controller parameters, ensuring a systematic and unbiased parameter selection process. Firstly, initial values that provide a stable system response are assigned. Each parameter is then updated to achieve the minimum settling time.

DOBC, UIO in DAC, and EID estimator methods recommend controller designs based on LQR or state feedback with pole placement methods, and their main controller parameters were determined using gradient descent. However, in the UDE method, the main controller is not a separate design like other methods. Instead, there are three design freedoms: filter, reference model, and error feedback gain, where the settling time of the reference model can be adjusted as desired. The last method, DUBRC, incorporates a robust controller design, where the sensitivity weighting filter bandwidth allows further reduction of settling time when there are no control input limitations.

To ensure fairness in comparison, the same optimization criterion—minimization of settling time—was applied to all methods. Additionally, identical filter parameters were used where applicable, and each controller was tuned according to the guidelines established in its original study.

$$\begin{aligned} y &= T(s)r \\ \underset{t_s}{\operatorname{argmin}}\, J(K_i, x, u, t) &= \|r - y\|_2 < 0.02 \\ &= \|r(1 - T(s, K_i))\|_2 < 0.02 \end{aligned} \tag{53}$$

The robust stability and robust performance criterion proven in Theorem 2 and 3 [17] is provided in (54) and (55), respectively.

The robust stability criterion:

$$\left\| W_T \tilde{T} \frac{S_{obs}}{1 - |W_T T_{obs}|} \right\|_\infty < 1 \tag{54}$$

where W_T is the uncertainty weight, $\tilde{T} \triangleq \tilde{G}C(1 + \tilde{G}C)^{-1}$ is the complementary sensitivity function, T_{obs} ($T_{obs} \triangleq GC_{obs}(1 + GC_{obs})^{-1} = 1 - S_{obs}$) the complementary sensitivity function of the observer and S_{obs} is the sensitivity function of the observer.

The robust performance criterion:

$$\left\| \frac{W_P \tilde{G} \tilde{S} S_{obs}}{1 - |W_T T_{obs}|} \right\|_\infty < 1 \tag{55}$$

where W_P is the performance weight, $\tilde{G}$ ($\tilde{G} \in \{G(1 + \Delta W_T) \mid \forall \|\Delta\|_\infty \leq 1\}$) is the perturbed plant (the real plant), $\tilde{S} \triangleq (1 + \tilde{G}C)^{-1}$ is the sensitivity function.

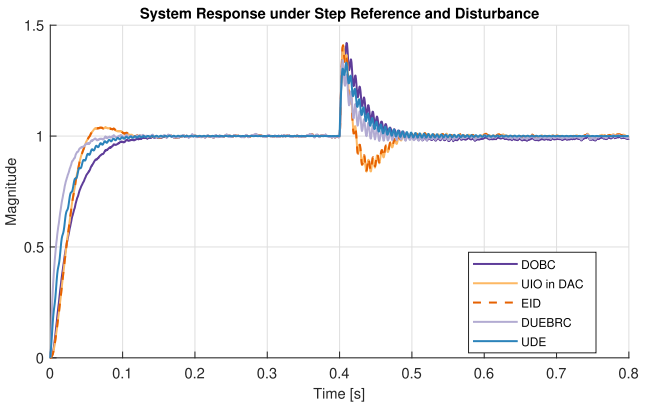

FIGURE 12. Step Responses under step disturbance with disturbance observer.

The system responses under step reference and step disturbance inputs are presented in Figure 12 for the methods designed when the disturbance observer structures are active, i.e., when the term $\hat{d}$ is integrated into the system. Specifically, the inputs are defined as $t = [0, \infty) \rightarrow r = 1$ and $t = [0.4, \infty) \rightarrow d = 1$. In contrast, Figure 13 illustrates the system responses under the same reference and disturbance inputs when the disturbance observer components are disabled, that is, when $\hat{d}$ is not integrated into the system.

The primary reason for the superior disturbance rejection performance of the UIO in DAC and EID methods, even

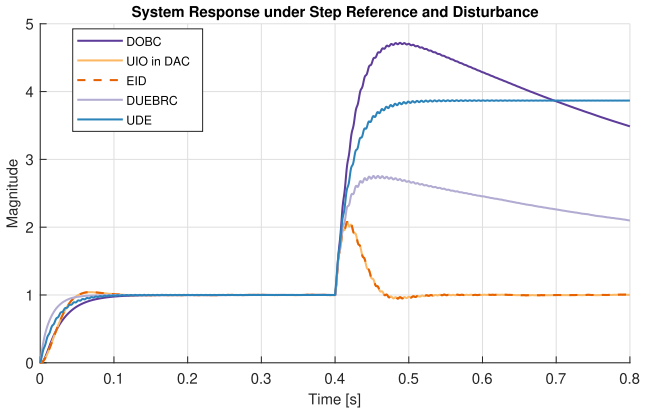

FIGURE 13. Step Responses under step disturbance without disturbance observer.

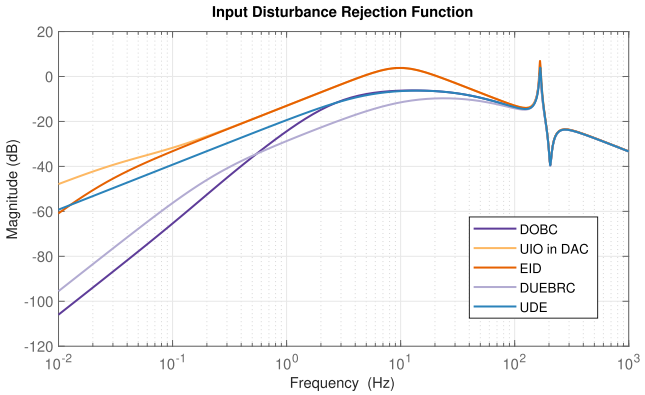

FIGURE 14. Input disturbance rejection functions.

when the disturbance observer is disabled, lies in their state observer structures. Furthermore, the disturbance observer methods' disturbance rejection performance, based on the design parameters obtained, is demonstrated in the frequency domain in Figure 14.

TABLE 2. Performance evaluation for reference tracking.

	DOBC	UIO in DAC	EID	DUEBRC	UDE
IAE	0.04897	0.04059	0.04023	0.03891	0.03544
ISE	0.02065	0.0191	0.01897	0.00879	0.0129

TABLE 3. Performance evaluation for estimation error.

	DOBC	UIO in DAC	EID	DUEBRC	UDE
IAE	0.02339	0.01735	0.0153	0.0535	0.01843
ISE	0.00293	0.00321	0.00304	0.00732	0.00282

To quantitatively assess the tracking and disturbance rejection capabilities of each control strategy, performance indices based on error signals are evaluated. The Integral Square Error (ISE) and Integral Absolute Error (IAE) for the reference tracking error corresponding to Figure 12 are presented in Table 2. Likewise, Table 3 provides the ISE and IAE values for the disturbance estimation error, computed as the difference between the actual and estimated disturbance signals.

G. COMPUTATIONAL COMPLEXITY EVALUATION

Table 4 provides a comparative analysis of the computational complexity for each disturbance observer-based control (DOBC) method to supplement the performance evaluation. The controller order is defined as the number of dynamic states involved in the closed-loop design, including estimators or augmentations. Average simulation time was measured in Simulink using the `tic-toc` timing functions over 10 trials with the `ode23tb` solver and a fixed simulation duration of 0.8 seconds.

TABLE 4. Computational complexity metrics for the five DOBC methods.

Method	Serial Block Depth	Avg. Sim. Time (s)
DOBC	5	1.455
UIO in DAC	5	1.181
EID	5	1.357
DUEBRC	7	0.815
UDE	5	2.768

Note: *Serial block depth reflects the order of individual dynamic elements but does not account for the number of serially connected blocks. Some methods may include more serial connections of low-order blocks, affecting simulation time.*

All methods except DUEBRC incorporate a common 5-state feedback structure derived from the plant model. DUEBRC employs a robust $\mathcal{H}_\infty$ design via LMI-based synthesis with augmented dynamics and additional filters, resulting in higher computational demand. Although Frequency Domain DOB has a fixed structure, its simulation time was comparatively higher, likely due to the use of model inversion and filtering under the solver dynamics. EID achieved the lowest simulation time, offering an effective trade-off between estimation performance and implementation efficiency. These results underline the trade-off between robustness and real-time implementability, which is critical in embedded control applications.

V. LIMITATION AND DIFFICULTIES

Before delving into the detailed limitations associated with DOBC methods, Table 5 provides an overview of the applicability of various DOBC approaches to different system types. This serves as a general reference to understand which methods are suitable for specific categories of systems. The subsequent subsections elaborate on the practical and theoretical challenges that may arise during implementation.

A. THEORETICAL CHALLENGES

While DOBC methods offer a systematic approach to achieving robust performance in uncertain environments, their practical implementation poses several theoretical and real-time challenges. First, most DOBC designs rely on

TABLE 5. Applicability of DOBC methods based on system types.

Methods	Minimum-Phase	Non-Minimum-Phase
FDOBC	Applicable	Modifications required
UIO in DAC	Applicable	Applicable
UDE	Applicable	Modifications required
EID	Applicable	Applicable
DUEBRC	Applicable	Applicable

accurate nominal models, which may not capture system nonlinearities, time delays, or unmodeled dynamics. This modeling mismatch directly affects the observer's ability to reconstruct disturbances accurately, particularly in nonlinear or time-varying systems [68]. Second, the tuning of observers in practice is non-trivial. Methods such as sliding mode observers or Kalman-based filters require trade-offs between responsiveness and noise sensitivity. Moreover, fast observer dynamics may amplify measurement noise, while slow dynamics reduce disturbance rejection capability [69]. Third, the computational cost of real-time observer-based control becomes more significant in embedded platforms. Algorithms must be optimized to ensure low-latency execution. In industrial applications such as grinding circuits or high-speed electric drives, disturbance observers need to be carefully designed to operate within sampling constraints and hardware limitations [69], [70]. These challenges motivate further research toward robust and adaptive observer architectures that can maintain estimation quality under practical constraints.

B. LIMITS OF THE ACTUATORS AND SENSORS

The actuators and sensors of electro-optical systems face limitations that vary by application and technology. The precision of the actuator is critical for small angular movements, while response time, maximum speed, accuracy, and repeatability affect the performance and stability of the system. Driver constraints also limit available frequency and power. For sensors, IMUs face noise issues, especially with low motion levels, and are prone to integration errors over time. High-frequency dynamic movements require IMUs with a wide bandwidth. The encoder resolution defines the accuracy of the position, and the accuracy and repeatability of the encoder significantly influence the position data, with IMU and encoder processing times that affect the control system's response.

C. MECHANICAL RESONANCES AND FLEXIBLE MODES

Mechanical resonance occurs when a system is excited at its natural frequency, causing resonance. In gimbal systems, mechanical components prone to vibrations at specific frequencies can lead to resonance. Flexible components can introduce flexible modes, especially in long, slender structures. Torsional mode frequencies and magnitudes influence gimbal dynamics and can be problematic in high-precision applications. Two types of resonance can occur: one due to torsional modes in the open-loop system, where sensor noise triggers resonance, which can be avoided by not driving the system at those frequencies. The second mode arises from external disturbances at the system's modal frequencies, requiring avoidance of overlap with the platform's modes. Failure to prevent these resonances can lead to system instability; although a bounded input-induced resonance will not make a stable system unstable, it can severely degrade performance.

D. STICK-SLIP / FRICTION EFFECTS

The stick-slip phenomenon, caused by friction, occurs in moving parts such as pan-tilt, gimbal, or inertial systems. It involves initial resistance (stiction), followed by sudden release and movement (slip); the stick-slip results from frictional forces, where friction is temporarily variable. The coefficient of friction, which determines the friction between surfaces, is a key factor in stick-slip behavior. Methods like adjusting friction, reducing surface irregularities, or using low-friction materials can be employed to prevent or reduce stick-slip, along with friction control strategies in system design.

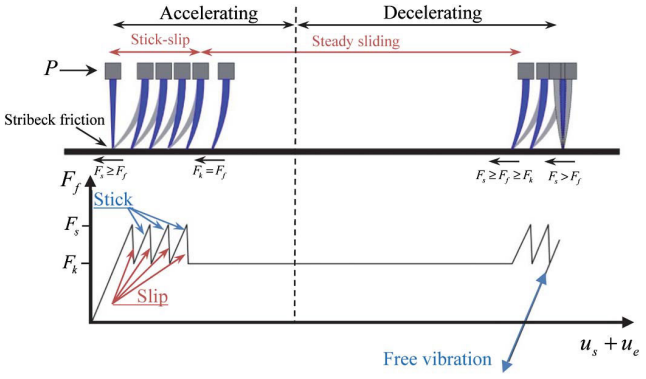

FIGURE 15. Illustration of the stick-slip phenomenon [71].

In the scenario described in [71] and illustrated in Figure 15, intermittent stick-slip occurs during sliding. A mass supported by a flexible mechanism, subjected to an increasing horizontal force, experiences cycles of sticking and slipping due to the interaction between static and kinetic friction. As the driving force increases, these cycles continue until a critical velocity is reached, after which steady sliding occurs. Ultimately, the mass and its supporting mechanics oscillate freely in their natural vibration period.

E. SOURCES OF DISTURBANCES AND UNCERTAINTIES

Disturbance sources in gimbal systems include external influences, mechanical vibrations, wind loads, and friction effects. Uncertainty arises from factors like mechanical tolerances, material variations, modeling errors, flex and cable spring effects, environmental conditions, and actuator/sensor sensitivities. High-frequency resonances are difficult to model, leaving this region uncertain, as measurements

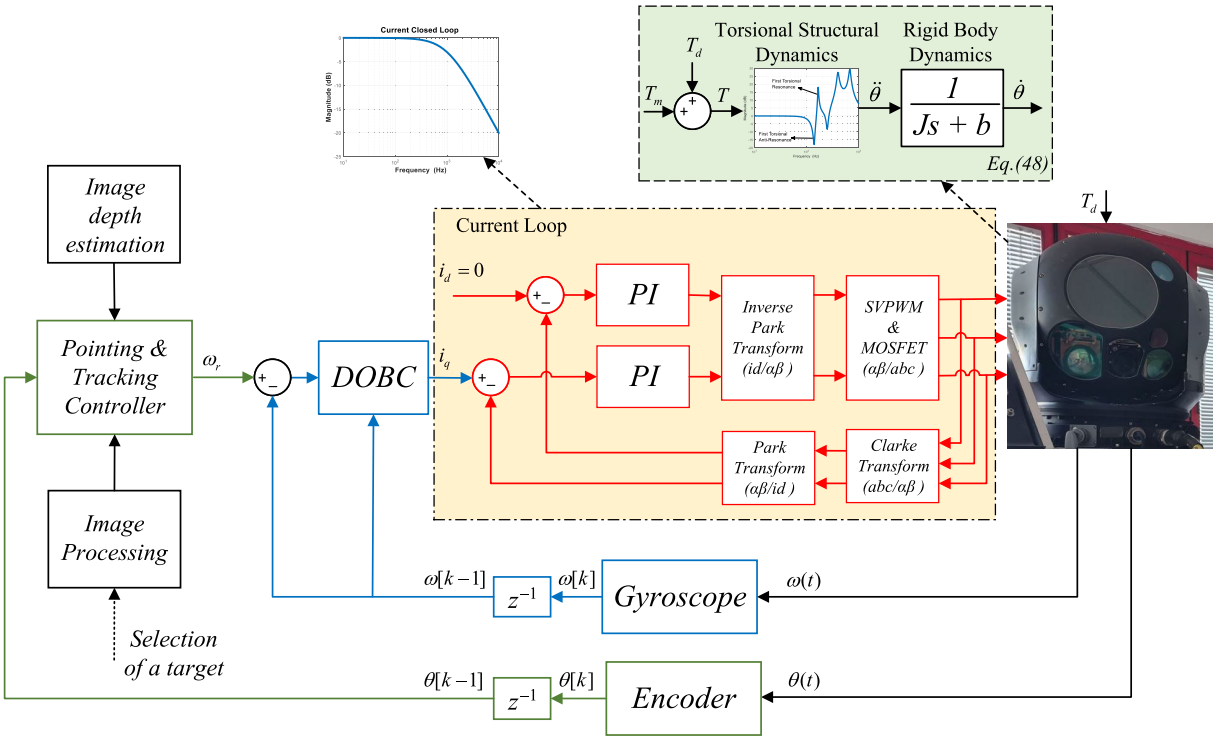

FIGURE 16. Schematic diagram of the gimbal system.

are limited by sensor bandwidth. Due to resistive and inductive uncertainties, current loops cannot act as fixed low-pass filters. As actuator torque frequency increases, PWM saturation occurs due to impedance, preventing sufficient drive for resonance modes. In summary, aside from sensor and actuator limits, high-frequency uncertainties also stem from production tolerances.

VI. EXPERIMENTAL VALIDATION

The system, whose experimental test environment is given in Figure 17, is capable of steering and precision stabilization. The gimbal system is driven by an alternating current (AC) motor to realize these high-performance functions. Designing and numerically implementing current, rate, and position control loops on the motor driver and processor board is possible. The motor current loop has a sampling frequency of at least 5 times the rate loop and has a high bandwidth. Thanks to the high PWM switching frequencies, the MOSFETs in the hardware are switched on and off. The system has an inertial measurement unit used for feedback in the rate loop. This sensor measures magnetic field, linear acceleration, and rotation. This measured feedback signal is input to the xPC target computer as analog via serial channel over the RS422 protocol with a 921,600 baud rate. Then it is read and converted into meaningful data by passing through Analog Digital Converters (ADC). Similarly, the feedback signals in the position loops are physically measured using a rotary encoder to make precise routing. Control algorithms are discretized and implemented at a sampling frequency of the rate loops is 2.5 kHz, since the IMU, which is used as feedback in the gyro loop, sends data at this frequency. Bilinear (bilinear) transformation, that is, "tustin" transformation, is preferred because it can be matched more accurately with continuous time. In this study, the signals are implemented in a 32-bit floating point format with 7.2 decimal digits of accuracy (24-bit). Then, 144 dB can be calculated as the signal-to-quantization-noise ratio. This suggests that it is safe to ignore quantization noise.

TABLE 6. System parameters.

Description	Value
Moment of inertia of the elevation axis J	$0.457\ kgm^2$
Viscous friction coefficient for elevation b	$2.56\ \frac{Nm}{rad/s}$
First torsional mode frequency ω_{c_r}	$1049\ \frac{rad}{s}$
First anti-resonance frequency $\omega_{c_{ar}}$	$1288\ \frac{rad}{s}$
Motor resistance R	$4.2\ \Omega$
Motor inductances $L_q = L_d$	$0.0068\ H$
Motor torque constant K_t	$1.08\ \frac{Nm}{A}$
Motor back EMF constant K_b	$1.08\ \frac{rad}{Vs}$

The parameter values of the Gimbal system used in the experimental test setup shown in Figure 17 are given in Table 6.

In the experimental test setup, the output of the DOBC, which is the control signal, is a current command. The motor is driven by a closed-loop current controller with a bandwidth

of approximately 1 kHz, producing torque in the system by multiplying this command by the motor's torque constant, K_t. For further details, refer to [72]. In this application, the DOBC methods are responsible for rejecting disturbances from the input channel and tracking the reference rate commands. The position loops form the outermost loop and serve multiple functions, including tracking position commands and performing tasks such as image-based automatic target tracking.

In this study, linear disturbance observer-based control methods are applied to two gimbal axes. Since this system is an electro-optic system, the payload of the system is cameras, electronic cards, and sensors. A schematic diagram of the gimbal is given in Figure 16.

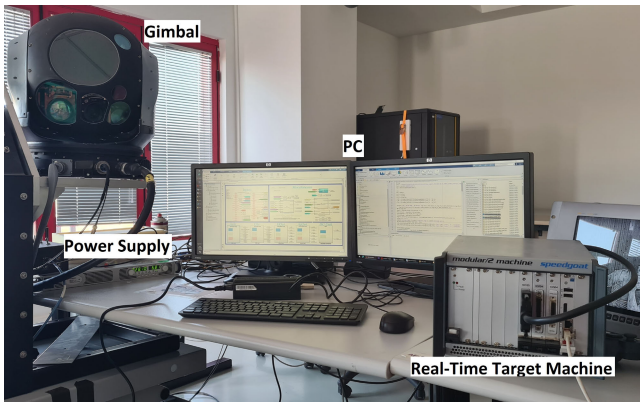

FIGURE 17. Experimental test setup.

As demonstrated in this study, DOBC methods can be applied to a 2-axis gimbal and adapted to the inner axes of a 4-axis gimbal.

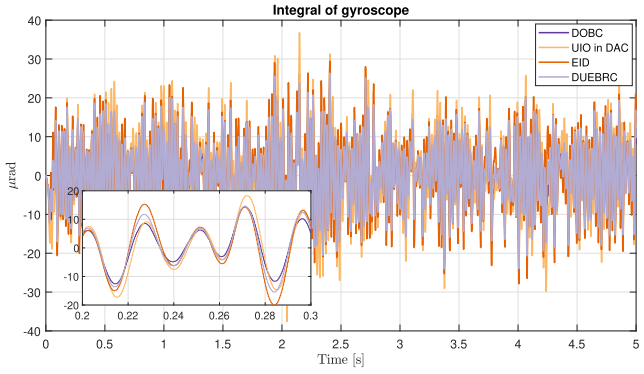

FIGURE 18. Integral of gyroscope under vibration.

The system responses given in Figure 18 and Figure 19 are the integral of the gyroscope and the gyroscope, affected by mass unbalance, gimbal transmissibility, friction, and bending effects when linear vibrations are applied to the stabilized axes of the gimbal. Gimbal transmissibility is a transfer function that varies according to the inertia matrix of the system and amplifies vibrations from the gimbal base

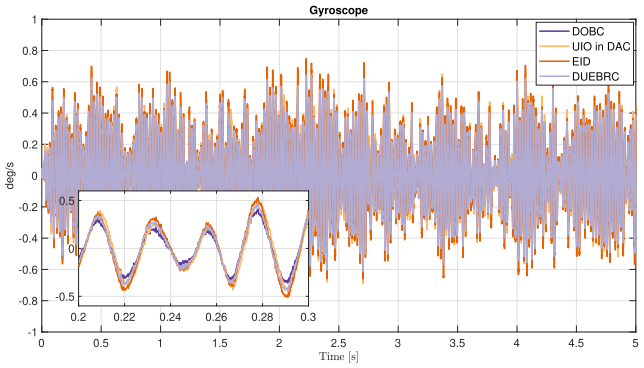

FIGURE 19. Gyroscope under vibration.

to the stabilized axis at certain frequencies. Mass unbalance converts linear acceleration effects, reflected on the stabilized axis, into disturbance torque along with the gimbal mass.

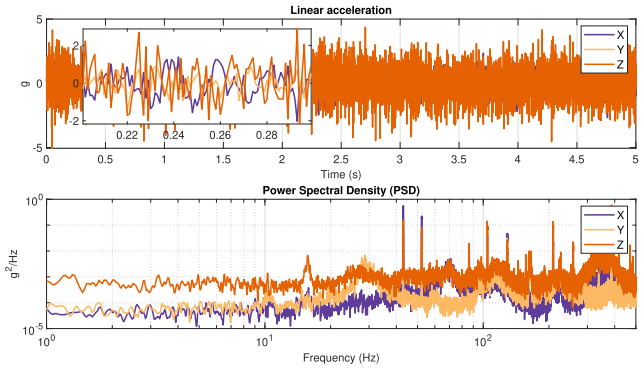

FIGURE 20. Linear acceleration time and frequency analysis.

The 3-axis time domain data and the power spectral density (PSD) frequency information of the platform vibrations, as shown in Figure 20, were applied to a 6-degree-of-freedom (DOF) motion simulation table. The axes are defined as follows: the x-axis corresponds to the front of the platform, the y-axis to the right side, and the z-axis is aligned with the direction of gravity. Disturbances were transmitted to the base of the gimbal according to the capacity and bandwidth limits of the motion simulation table.

The control system design and simulations presented in this study were performed using MATLAB R2024b. The workstation used had the following specifications: Windows 11 (64-bit) operating system, Intel Core i7-10510U CPU, and 16 GB of RAM. These specifications ensured the computational feasibility of designing and simulating DOBC methods without significant performance limitations.

VII. CONCLUSION

In this paper, the theoretical foundations of commonly used DOBC methods in the literature, along with their expressions in the time and frequency domains, have been discussed. Various assumptions compatible with the problem were stated to obtain meaningful comparative results and

express the problem definitions given by the pioneers of the methods in an equivalent form. Along with these assumptions, the DOBC methods specified with different state-space representations have been made applicable to the same disturbance-input signals.

A comparative analysis of structures for the simulation environment designed for an electro-optical gimbal system was presented, and various metrics were shared to select a system-specific DOBC method and potential improvement methods. In addition to simulations, an experimental implementation was performed. Disturbance input signals covering a wide spectrum were applied to the real system using a six-degree-of-freedom motion simulation platform. An experimental comparison of DOBC methods is highlighted, and a notable gap in the literature is identified. However, it is important to note that the effectiveness of each method is dependent on system-specific characteristics, and the conclusions drawn in this study may vary for different applications. While efforts were made to ensure a fair and unbiased evaluation, factors such as hardware limitations, tuning sensitivities, and real-time computational constraints may influence practical outcomes.

In particular, the limits of systems that perform well theoretically have been revealed in experimental applications, providing a valuable perspective for engineers dealing with practical aspects. Despite careful tuning, some methods exhibited performance degradation in real-time implementations due to unmodeled nonlinearities, actuator saturation, and sensor limitations. Additionally, some DOBC methods are more sensitive to parameter variations, requiring extensive tuning to maintain stability and robustness under different conditions.

Determining the total disturbance torque is challenging in practical applications. Therefore, it is possible to discuss the components that contribute to this torque. Ultimately, the DOBC is used to estimate these disturbances in real-time. In addition to the UDE method, other methods provide results in real-time applications similar to simulation. In contrast, the UDE method does not yield successful results despite using estimated values with Kalman and Luenberger observer methods in real-time. This highlights another challenge: while simulation results may indicate promising performance, certain DOBC methods may struggle with real-world uncertainties and high-frequency disturbances that were not fully captured in the simulation model.

Due to unmodeled components of the physical system, a very high bandwidth is not achievable. To ensure no stability difference between simulation and reality, the simulation environment's design should consider the physical constraints of the actual system. Model uncertainties are addressed by modeling them, and retroactive design updates are made to analyze and solve problems that may be encountered in reality, minimizing differences between simulation and reality to proceed with the process. However, despite these efforts, small discrepancies between simulation and real-world implementation remain inevitable, particularly in high-frequency disturbance rejection and extreme operating conditions.

REFERENCES

[1] T. Fortier and E. Baumann, "20 years of developments in optical frequency comb technology and applications," *Commun. Phys.*, vol. 2, no. 1, pp. 1–16, Dec. 2019.

[2] P. I. Corke and M. C. Good, "Dynamic effects in visual closed-loop systems," *IEEE Trans. Robot. Autom.*, vol. 12, no. 5, pp. 671–683, Feb. 1996.

[3] L.-L. Xie and L. Guo, "How much uncertainty can be dealt with by feedback?" *IEEE Trans. Autom. Control*, vol. 45, no. 12, pp. 2203–2217, Dec. 2000.

[4] B. Kürkçü and M. Tomizuka, "Algebraic control: Complete stable inversion with necessary and sufficient conditions," 2024, *arXiv:2501.00172*.

[5] H. Shim, G. Park, Y. Joo, J. Back, and N. H. Jo, "Yet another tutorial of disturbance observer: Robust stabilization and recovery of nominal performance," *Control Theory Technol.*, vol. 14, no. 3, pp. 237–249, Aug. 2016.

[6] K. Ohishi, M. Nakao, K. Ohnishi, and K. Miyachi, "Microprocessor-controlled DC motor for load-insensitive position servo system," *IEEE Trans. Ind. Electron.*, vol. IE-34, no. 1, pp. 44–49, Feb. 1987.

[7] C. Johnson, "Accomodation of external disturbances in linear regulator and servomechanism problems," *IEEE Trans. Autom. Control*, vol. AC-16, no. 6, pp. 635–644, Dec. 1971.

[8] S. Li, J. Yang, W.-H. Chen, and X. Chen, *Disturbance Observer-Based Control: Methods and Applications*. Boca Raton, FL, USA: CRC Press, 2014.

[9] T. Bünte, D. Odenthal, B. Aksun-Güvenç, and L. Güvenç, "Robust vehicle steering control design based on the disturbance observer," *Annu. Rev. Control*, vol. 26, no. 1, pp. 139–149, Jan. 2002.

[10] K. Natori, R. Oboe, and K. Ohnishi, "Stability analysis and practical design procedure of time delayed control systems with communication disturbance observer," *IEEE Trans. Ind. Informat.*, vol. 4, no. 3, pp. 185–197, Aug. 2008.

[11] S. Yu and M. Tomizuka, "Performance enhancement of iterative learning control system using disturbance observer," in *Proc. IEEE/ASME Int. Conf. Adv. Intell. Mechatronics*, Jul. 2009, pp. 987–992.

[12] A. Bayrak, B. Kürkçü, and M. Ö. Efe, "A new adaptive disturbance/uncertainty estimator based control scheme for LTI systems," *IEEE Access*, vol. 10, pp. 106849–106858, 2022.

[13] A. Alan, T. G. Molnar, E. Das, A. D. Ames, and G. Orosz, "Disturbance observers for robust safety-critical control with control barrier functions," *IEEE Control Syst. Lett.*, vol. 7, pp. 1123–1128, 2023.

[14] X. Wang, S. Li, X. Yu, and J. Yang, "Distributed active anti-disturbance consensus for leader-follower higher-order multi-agent systems with mismatched disturbances," *IEEE Trans. Autom. Control*, vol. 62, no. 11, pp. 5795–5801, Nov. 2017.

[15] A. Mohammadi, H. J. Marquez, and M. Tavakoli, "Nonlinear disturbance observers: Design and applications to Euler–Lagrange systems," *IEEE Control Syst. Mag.*, vol. 37, no. 4, pp. 50–72, Aug. 2017.

[16] B. Kürkçü, C. Kasnakoglu, and M. Ö. Efe, "Disturbance/uncertainty estimator based integral sliding-mode control," *IEEE Trans. Autom. Control*, vol. 63, no. 11, pp. 3940–3947, Nov. 2018.

[17] B. Kürkçü, C. Kasnakoglu, and M. Ö. Efe, "Disturbance/uncertainty estimator based robust control of nonminimum phase systems," *IEEE/ASME Trans. Mechatronics*, vol. 23, no. 4, pp. 1941–1951, Aug. 2018.

[18] H. Shim and N. H. Jo, "An almost necessary and sufficient condition for robust stability of closed-loop systems with disturbance observer," *Automatica*, vol. 45, no. 1, pp. 296–299, Jan. 2009.

[19] A. T. Vo, T. N. Truong, and H.-J. Kang, "A novel tracking control algorithm with finite-time disturbance observer for a class of second-order nonlinear systems and its applications," *IEEE Access*, vol. 9, pp. 31373–31389, 2021.

[20] W. Zhang, M. Tomizuka, P. Wu, Y.-H. Wei, Q. Leng, S. Han, and A. K. Mok, "A double disturbance observer design for compensation of unknown time delay in a wireless motion control system," *IEEE Trans. Control Syst. Technol.*, vol. 26, no. 2, pp. 675–683, Mar. 2018.

[21] B. Kürkçü and C. Kasnakoglu, "Robust autopilot design based on a disturbance/uncertainty/coupling estimator," *IEEE Trans. Control Syst. Technol.*, vol. 27, no. 6, pp. 2622–2629, Nov. 2019.

[22] J. R. S. Benevides, M. A. D. Paiva, P. V. G. Simplício, R. S. Inoue, and M. H. Terra, "Disturbance observer-based robust control of a quadrotor subject to parametric uncertainties and wind disturbance," *IEEE Access*, vol. 10, pp. 7554–7565, 2022.

[23] M. Korda and I. Mezić, "Linear predictors for nonlinear dynamical systems: Koopman operator meets model predictive control," *Automatica*, vol. 93, pp. 149–160, Jul. 2018.

[24] C. Ren, H. Jiang, C. Li, W. Sun, and S. Ma, "Koopman-operator-based robust data-driven control for wheeled mobile robots," *IEEE/ASME Trans. Mechatronics*, vol. 28, no. 1, pp. 461–472, Feb. 2023.

[25] S. N. Dashkovskiy, D. V. Efimov, and E. D. Sontag, "Input to state stability and allied system properties," *Autom. Remote Control*, vol. 72, no. 8, pp. 1579–1614, Aug. 2011.

[26] M. Hirao, B. Kurkcu, A. Ghanbarpour, and M. Tomizuka, "Frequency domain analysis of nonlinear series elastic actuator via describing function," in *Proc. IEEE Int. Conf. Robot. Biomimetics (ROBIO)*, Dec. 2023, pp. 1–6.

[27] P. Bieber, F. Boniol, M. Boyer, E. Noulard, and C. Pagetti, "New challenges for future avionic architectures," *Aerosp. Lab*, vol. 4, no. 4, pp. 1–11, 2012.

[28] Z. Hurak and M. Rezac, "Image-based pointing and tracking for inertially stabilized airborne camera platform," *IEEE Trans. Control Syst. Technol.*, vol. 20, no. 5, pp. 1146–1159, Sep. 2012.

[29] J. Hilkert, "Inertially stabilized platform technology concepts and principles," *IEEE Control Syst. Mag.*, vol. 28, no. 1, pp. 26–46, Jan. 2008.

[30] M. Özçelik, B. Kürkçü, and Z. Y. Bayraktaroğlu, "Experimental comparison of H-infinity synthesis and feedback linearization on a MIMO gimbal example," in *Proc. IEEE Conf. Control Technol. Appl. (CCTA)*, Aug. 2023, pp. 984–991.

[31] W. Ren, Q. Qiao, K. Nie, and Y. Mao, "Robust DOBC for stabilization loop of a two-axes gimbal system," *IEEE Access*, vol. 7, pp. 110554–110562, 2019.

[32] L. Zhang, H. Nan, Z. Zhao, and Y. Yuan, "Adaptive disturbance observer-based dual-loop integral-type fast terminal sliding mode control for micro spacecraft and its gimbal tracking device," *ISA Trans.*, vol. 130, pp. 121–135, Nov. 2022. [Online]. Available: https://www.sciencedirect.com/science/article/pii/S0019057822001306

[33] Y. Yang, Y. Cui, J. Qiao, and Y. Zhu, "Adaptive periodic-disturbance observer based composite control for SGCMG gimbal servo system with rotor vibration," *Control Eng. Pract.*, vol. 132, Mar. 2023, Art. no. 105407. [Online]. Available: https://www.sciencedirect.com/science/article/pii/S0967066122002386

[34] Y. Cui, Y. Yang, L. Zhao, Y. Zhu, J. Qiao, and L. Guo, "Composite control for gimbal systems with multiple disturbances: Analysis, design, and experiment," *IEEE Trans. Syst., Man, Cybern., Syst.*, vol. 53, no. 8, pp. 4789–4798, 2023, doi: 10.1109/TSMC.2023.3257860.

[35] W.-H. Chen, J. Yang, L. Guo, and S. Li, "Disturbance-observer-based control and related methods—An overview," *IEEE Trans. Ind. Electron.*, vol. 63, no. 2, pp. 1083–1095, Feb. 2016.

[36] J.-H. She, M. Fang, Y. Ohyama, H. Hashimoto, and M. Wu, "Improving disturbance-rejection performance based on an equivalent-input-disturbance approach," *IEEE Trans. Ind. Electron.*, vol. 55, no. 1, pp. 380–389, Jan. 2008.

[37] Q.-C. Zhong, A. Kuperman, and R. K. Stobart, "Design of UDE-based controllers from their two-degree-of-freedom nature," *Int. J. Robust Nonlinear Control*, vol. 21, no. 17, pp. 1994–2008, Nov. 2011.

[38] J. Han, "From PID to active disturbance rejection control," *IEEE Trans. Ind. Electron.*, vol. 56, no. 3, pp. 900–906, Mar. 2009.

[39] C. Johnson, "Further study of the linear regulator with disturbances—The case of vector disturbances satisfying a linear differential equation," *IEEE Trans. Autom. Control*, vol. AC-15, no. 2, pp. 222–228, Apr. 1970.

[40] Z. Gao, "Scaling and bandwidth-parameterization based controller tuning," in *Proc. Amer. Control Conf.*, vol. 6, 2006, pp. 4989–4996.

[41] W. Chen, "Disturbance observer based control for nonlinear systems," *IEEE/ASME Trans. Mechatronics*, vol. 9, no. 4, pp. 706–710, Apr. 2004.

[42] B.-Z. Guo and Z.-L. Zhao, *Active Disturbance Rejection Control for Nonlinear Systems: An Introduction*. Hoboken, NJ, USA: Wiley, 2017.

[43] K. Rsetam, Y. Zheng, Z. Cao, and Z. Man, "Adaptive active disturbance rejection control for vehicle steer-by-wire under communication time delays," *Appl. Syst. Innov.*, vol. 7, no. 2, p. 22, Mar. 2024. [Online]. Available: https://www.mdpi.com/2571-5577/7/2/22

[44] K. Rsetam, Z. Cao, Z. Man, and X.-M. Zhang, "GPIO-based continuous sliding mode control for networked control systems under communication delays with experiments on servo motors," *IEEE/CAA J. Autom. Sinica*, vol. 12, no. 1, pp. 99–113, Jan. 2025. [Online]. Available: https://www.ieee-jas.net/en/article/doi/10.1109/JAS.2024.124812

[45] K. Rsetam, Z. Cao, and Z. Man, "Cascaded-extended-state-observer-based sliding-mode control for underactuated flexible joint robot," *IEEE Trans. Ind. Electron.*, vol. 67, no. 12, pp. 10822–10832, Dec. 2020.

[46] J. Yang, W.-H. Chen, and S. Li, "Non-linear disturbance observer-based robust control for systems with mismatched disturbances/uncertainties," *IET Control Theory Appl.*, vol. 5, no. 18, pp. 2053–2062, Dec. 2011.

[47] X. Liu, H. Yu, J. Yu, and L. Zhao, "Combined speed and current terminal sliding mode control with nonlinear disturbance observer for PMSM drive," *IEEE Access*, vol. 6, pp. 29594–29601, 2018.

[48] K. Zhou and J. C. Doyle, *Essentials of Robust Control*, vol. 104. Upper Saddle River, NJ, USA: Prentice-Hall, 1998.

[49] B. Kürkçü, C. Kasnakoğlu, M. Ö. Efe, and R. Su, "On the existence of equivalent-input-disturbance and multiple integral augmentation via H-infinity synthesis for unmatched systems," *ISA Trans.*, vol. 131, pp. 299–310, Dec. 2022.

[50] N. H. Jo, H. Shim, and Y. I. Son, "Disturbance observer for non-minimum phase linear systems," *Int. J. Control, Autom. Syst.*, vol. 8, no. 5, pp. 994–1002, Oct. 2010.

[51] L. Wang and J. Su, "Disturbance rejection control for non-minimum phase systems with optimal disturbance observer," *ISA Trans.*, vol. 57, pp. 1–9, Jul. 2015.

[52] H. Chang, H. Kim, and H. Shim, "Lemmas on determination of minimum bandwidth of Q-filter for robust stability of feedback loop with disturbance observers," in *Proc. 59th IEEE Conf. Decis. Control (CDC)*, Dec. 2020, pp. 893–898.

[53] A. Tesfaye, H. Seong Lee, and M. Tomizuka, "A sensitivity optimization approach to design of a disturbance observer in digital motion control systems," *IEEE/ASME Trans. Mechatronics*, vol. 5, no. 1, pp. 32–38, Mar. 2000.

[54] Q. Liu, M. Liu, Q. Jin, and Y. Liu, "Design of DOB-based control system in the presence of uncertain delays for low-order processes," *IEEE Trans. Control Syst. Technol.*, vol. 28, no. 2, pp. 558–565, Mar. 2020.

[55] M. Ö. Efe and C. Kasnakoğlu, "An enhanced bandwidth disturbance observer based control–S-filter approach," *TURKISH J. Electr. Eng. Comput. Sci.*, vol. 29, no. 4, pp. 2170–2185, Jul. 2021.

[56] M. Elkayam, S. Kolesnik, and A. Kuperman, "Guidelines to classical frequency-domain disturbance observer redesign for enhanced rejection of periodic uncertainties and disturbances," *IEEE Trans. Power Electron.*, vol. 34, no. 4, pp. 3986–3995, Apr. 2019.

[57] J. Han, H. Kim, Y. Joo, N. H. Jo, and J. H. Seo, "A simple noise reduction disturbance observer and Q-filter design for internal stability," in *Proc. 13th Int. Conf. Control, Autom. Syst. (ICCAS)*, Oct. 2013, pp. 755–760.

[58] J. Schoukens, R. Pintelon, E. van der Ouderaa, and J. Renneboog, "Survey of excitation signals for FFT based signal analyzers," *IEEE Trans. Instrum. Meas.*, vol. 37, no. 3, pp. 342–352, Mar. 1988.

[59] Q.-C. Zhong and D. Rees, "Control of uncertain LTI systems based on an uncertainty and disturbance estimator," *J. Dyn. Syst., Meas., Control*, vol. 126, no. 4, pp. 905–910, Dec. 2004.

[60] Y. Wang, B. Ren, and Q.-C. Zhong, "Bounded UDE-based controller for input constrained systems with uncertainties and disturbances," *IEEE Trans. Ind. Electron.*, vol. 68, no. 2, pp. 1560–1570, Feb. 2021.

[61] R. K. Stobart, A. Kuperman, and Q.-C. Zhong, "Uncertainty and disturbance estimator–based control for uncertain LTI-SISO systems with state delays," *J. Dyn. Syst., Meas., Control*, vol. 133, no. 2, Feb. 2011, Art. no. 024502, doi: 10.1115/1.4003265.

[62] L. Sun, D. Li, Q.-C. Zhong, and K. Y. Lee, "Control of a class of industrial processes with time delay based on a modified uncertainty and disturbance estimator," *IEEE Trans. Ind. Electron.*, vol. 63, no. 11, pp. 7018–7028, Nov. 2016.

[63] Y. Zhang, L. Sun, J. Shen, K. Y. Lee, and Q.-C. Zhong, "Iterative tuning of modified uncertainty and disturbance estimator for time-delay processes: A data-driven approach," *ISA Trans.*, vol. 84, pp. 164–177, Jan. 2019.

[64] M. Abdo, A. R. Vali, A. Toloei, and M. R. Arvan, "Research on the cross-coupling of a two axes gimbal system with dynamic unbalance," *Int. J. Adv. Robotic Syst.*, vol. 10, no. 10, p. 357, Oct. 2013.

[65] G. Özdoğan and K. Leblebicioğlu, "Frequency response function measurement and parametric SISO system modelling of a gyro-stabilized infrared electro optic gimbal system," *Trans. Inst. Meas. Control*, vol. 38, no. 5, pp. 512–528, May 2016.
[66] K. Lewotsky. (2015). *Tutorial: Understanding the Mysteries of Inertia Mismatch*. [Online]. Available: https://www.automate.org/industry-insights/understanding-the-mysteries-of-inertia-mismatch
[67] E. Dincel and M. T. Söylemez, "Limitations on dominant pole pair selection with continuous PI and PID controllers," in *Proc. Int. Conf. Control, Decis. Inf. Technol. (CoDIT)*, Apr. 2016, pp. 741–745.
[68] H. Ren, H. Ma, H. Li, and R. Lu, "A disturbance observer based intelligent control for nonstrict-feedback nonlinear systems," *Sci. China Technological Sci.*, vol. 66, no. 2, pp. 456–467, Feb. 2023.
[69] B. Xu, L. Zhang, and W. Ji, "Improved non-singular fast terminal sliding mode control with disturbance observer for PMSM drives," *IEEE Trans. Transport. Electrific.*, vol. 7, no. 4, pp. 2753–2762, Dec. 2021.
[70] H. Khodadadi and H. Ghadiri, "Fuzzy logic self-tuning PID controller design for ball mill grinding circuits using an improved disturbance observer," *Mining, Metall. Explor.*, vol. 36, no. 6, pp. 1075–1090, Dec. 2019.
[71] F. Nikfar and D. Konstantinidis, "Effect of the stick-slip phenomenon on the sliding response of objects subjected to pulse excitation," *J. Eng. Mech.*, vol. 143, no. 4, Apr. 2017, Art. no. 04016122.
[72] G. Özdogan and K. Leblebicioglu, "Cogging torque disturbance rejection for a low-cost gimbal motor and a controller design with practical considerations," in *Proc. 12th Asian Control Conf. (ASCC)*, Jun. 2019, pp. 486–491.

MÜCAHİD RIDVAN KAPLAN received the B.Sc. degree from the Department of Control and Automation Engineering, Istanbul Technical University, in 2019, and the M.Sc. degree from the System Dynamics and Control Program, Department of Mechanical Engineering, Istanbul Technical University, in 2022. He is currently pursuing the Ph.D. degree with the Department of Computer Engineering, Hacettepe University. He is also a Lead Control Systems Design Engineer with Aselsan Inc. His research interests include dynamical system modeling and simulation and control theory, with applications to the aerospace industry.

BURAK KÜRKÇÜ (Member, IEEE) received the B.Sc. degree from Istanbul Technical University, in 2010, and the M.Sc. and Ph.D. degrees from the Department of Electrical and Electronics Engineering, TOBB University of Economics and Technology, in 2015 and 2019, respectively.

He is currently an Assistant Professor with the Department of Electrical and Computer Engineering, Santa Clara University (SCU), CA, USA. Before joining SCU, he was a Research Scholar with UC Berkeley, for two years, and held various academic and industrial roles with Hacettepe University and Aselsan Inc. He has authored or co-authored several notable publications in these fields. His research focuses on control theory and robotics applications. He received the IEEE Türkiye Ph.D. Thesis Award, in 2020. He is an Associate Editor of *Transactions of the Institute of Measurement and Control*, *Measurement and Control*, and the *Turkish Journal of Electrical Engineering and Computer Science*.

MEHMET ÖNDER EFE (Senior Member, IEEE) received the B.S. degree from the Department of Electronics and Communications Engineering, Istanbul Technical University, Istanbul, Türkiye, in 1993, the M.S. degree from the Department of Systems and Control Engineering, Boğaziçi University, Istanbul, in 1996, and the Ph.D. degree from the Department of Electrical and Electronics Engineering, Boğaziçi University, in 2000.

He is currently with the Department of Computer Engineering, Hacettepe University, Ankara, Türkiye. He is/was an Editor/Associate Editor of IEEE TRANSACTIONS ON ARTIFICIAL INTELLIGENCE, IEEE TRANSACTIONS ON INDUSTRIAL ELECTRONICS, IEEE TRANSACTIONS ON INDUSTRIAL INFORMATICS, IEEE/ASME TRANSACTIONS ON MECHATRONICS, *Transactions of the Institute of Measurement and Control*, and *Measurement and Control*.

ZEKİ YAĞIZ BAYRAKTAROĞLU received the B.Sc. degree from the Department of Mechanical Engineering, Istanbul Technical University, Türkiye, in 1997, the M.Sc. degree from the Department of Mechanical Engineering, Arts et Metiers ParisTech, in 1998, and the Ph.D. degree from the Department of Mechanical Engineering, University of Versailles Saint-Quentin-en-Yvelines, in 1998. He is currently an Associate Professor with the Department of Mechanical Engineering, Istanbul Technical University.